Title: ATRAID, a genetic factor that regulates the action of nitrogen-containing bisphosphonates on bone

Authors: Lauren E. Surface[1], Jiwoong Park[2], Sandeep Kumar[2], Damon T. Burrow[2], Cheng Lyu[2], Jinmei Li[2], Niki Song[2], Zhou Yu[1], Abbhirami Rajagopal[3,#], Yangjin Bae[3], Brendan H. Lee[3], Steven Mumm[4], Gabe Haller[5], Charles C. Gu[6], Jonathan C. Baker[7], Mahshid Mohseni[4], Melissa Sum[8], Margaret Huskey[4], Shenghui Duan[4], Vinieth N. Bijanki[9], Roberto Civitelli[4], Michael J. Gardner[10], Chris M. McAndrew[5], William M. Ricci[11], Christina A. Gurnett[5], Kathryn Diemer[4], Jan E. Carette[12], Malini Varadarajan[13,*], Thijn R. Brummelkamp[13], Kivanc Birsoy[14], David M. Sabatini[15-17], Timothy R. Peterson[2]*

Affiliations:
[1] Department of Molecular and Cellular Biology, Department of Chemistry and Chemical Biology, Faculty of Arts and Sciences Center for Systems Biology, Harvard University, Cambridge, MA 02138, USA.
[2] Division of Bone & Mineral Diseases, Department of Internal Medicine, Department of Genetics, Institute for Public Health, Washington University School of Medicine, BJC Institute of Health, 425 S. Euclid Ave., St. Louis, MO 63110, USA.
[3] Department of Molecular and Human Genetics, Baylor College of Medicine, Houston, TX, 77030, USA.
[#] (present address) Harris County Public health, Houston, TX, 77027, USA.
[4] Division of Bone & Mineral Diseases, Department of Internal Medicine, Washington University School of Medicine, BJC Institute of Health, 425 S. Euclid Ave., St. Louis, MO 63110, USA.
[5] Department of Orthopedic Surgery, Washington University School of Medicine, 4938 Parkview Place, St. Louis, MO 63110, USA.
[6] Division of Biostatistics, Washington University School of Medicine, 660 S. Euclid Ave., CB 8067, St. Louis, MO 63110-1093, USA.
[7] Mallinckrodt Institute of Radiology, Washington University School of Medicine, 510 S. Kingshighway Blvd. Louis, MO 63110, USA.
[8] Division of Endocrinology, Diabetes and Metabolism, NYU Langone Health, 530 1st Ave., Schwartz 5E. New York, NY 10016, USA.
[9] Center for Metabolic Bone Disease and Molecular Research, Shriners Hospital for Children, St. Louis, MO 63110, USA.
[10] Stanford University, Department of Orthopedic Surgery, 450 Broadway Street, Redwood City, CA 94063-6342, USA.
[11] Hospital for Special Surgery Main Campus - Belaire Building, 525 East 71st Street 2nd Floor, New York, NY 10021, USA.
[12] Department of Microbiology and Immunology, Stanford University School of Medicine, Stanford, CA 94305, USA.
[13] Netherlands Cancer Institute, Amsterdam, The Netherlands.
[*] (present address) Developmental and molecular pathways, Novartis institutes for biomedical research, Cambridge, CA 02140, USA.
[14] The Rockefeller University, 1230 York Ave, New York 10065, USA.
[15] Whitehead Institute, 9 Cambridge Center, Cambridge, MA 02139, USA.
[16] Department of Biology, Massachusetts Institute of Technology (MIT), 77 Massachusetts Avenue, Cambridge, MA 02139, USA.
[17] David H. Koch Center for Integrative Cancer Research at MIT, 77 Massachusetts Avenue, Cambridge, MA 02139, USA.
Corresponding author:[::] * timrpeterson@wustl.edu (T.R.P).

One Sentence Summary: The identification of the gene, *ATRAID*, essential for responses to the commonly prescribed osteoporosis drugs, nitrogen-containing bisphosphonates.

Abstract:

Nitrogen-containing bisphosphonates (N-BPs), such as alendronate (Fosamax®), are the mostly widely prescribed medications for diseases involving bone (*1-3*), with nearly 200 million prescriptions written annually. In the last few years, widespread use of N-BPs has been challenged due to the risk of rare but significant side effects such as atypical femoral fractures (AFF) and osteonecrosis of the jaw (ONJ) (*4-7*). N-BPs bind to and inhibit farnesyl diphosphate synthase (FDPS), resulting in defects in protein prenylation (*8-10*). Yet it remains poorly understood what other cellular factors might allow N-BPs to exert their pharmacological effects. Herein, we perform genome-wide studies in cells and patients to identify the poorly characterized gene, *ATRAID*. Loss of *ATRAID* function results in selective resistance to N-BP-mediated loss of cell viability and the prevention of alendronate-mediated inhibition of prenylation. *ATRAID* is required for alendronate inhibition of osteoclast function, and *ATRAID*-deficient mice have impaired therapeutic responses to alendronate in a model of postmenopausal osteoporosis. Lastly, we performed exome sequencing on osteoporosis patients taking N-BPs that did or did not suffer an AFF. *ATRAID* is one of five genes that contains rare non-synonymous coding variants in the AFF patients that is also differentially expressed in poor outcome groups of cancer patients treated with N-BPs. Our work adds key insight into the mechanistic action of N-BPs and the processes that might underlie differential responsiveness to N-BPs in people.

INTRODUCTION

Nitrogen-containing bisphosphonates (N-BPs) are the standard treatment for osteoporosis and several other bone diseases (*11, 12*). Certain N-BPs (pamidronate (Aredia®), zoledronate (Zometa®)) are also routinely prescribed to prevent skeletal complications in patients with multiple myeloma and with bone metastases from other malignancies, including breast and prostate cancer (*13*). However, because N-BPs cause rare yet serious side-effects, such as atypical fractures and osteonecrosis of the jaw, many patients avoid taking them (*5-7, 11*), causing the number of prescriptions to plummet over 50% in the last decade (*7, 14*). A plan for addressing this crisis, developed by American Society for Bone and Mineral Research (ASBMR) leadership, calls for better pharmacogenomics to identify genetic factors that may underlie response to this class of drugs (*7*).

A goal of personalized medicine is to identify biomarkers that underlie drug responsiveness. In the case of the N-BPs, it can be said that there are limited personalization options owing to the limited number of genes implicated in the pharmacologic effects of N-BPs. Exposure of cells to N-BPs leads to inhibition of farnesyl diphosphate synthase (FDPS, a.k.a., FPPS) resulting in reduction in protein prenylation (*15*). Based on this observation, it is widely believed that N-BPs act therapeutically by impairing protein prenylation, ultimately leading to deficits in numerous cellular processes including differentiation, recruitment, and adhesion of osteoclasts (the major bone resorptive cell type) to bone and/or osteoclast cell death (*16-18*). Recently we performed CRISPRi-based, genome-wide screening and identified a poorly characterized gene, *SLC37A3,* that provides molecular details for how the N-BPs reach their target, FDPS (*19*). As part of that work we determined that SLC37A3 requires another poorly characterized protein, ATRAID, for its expression (*19*). In this work, we independently identified *ATRAID* using a different genome-wide, mutagenesis strategy. We generated *ATRAID* deficient mice and determined that it is required for the regulation of N-BPs on bone. We also performed exome sequencing in

osteoporotic patients and identified rare coding variants in *ATRAID* in patients that suffered atypical fractures while taking N-BPs.

RESULTS

ATRAID is required for molecular responses to nitrogen-containing bisphosphonates

To provide insight into the mechanism(s) of N-BPs action, we performed a genetic screen to identify human genes required for the anti-proliferative effects of N-BPs (Fig. 1A). We made use of a largely haploid human cell line of myeloid origin (KBM7, a.k.a. HAP1) to generate a library of retroviral gene trap mutants (*20*), and then selected for clones which are resistant to cytotoxic levels of alendronate. The advantages of this cell line for genetic screening include: 1) each gene is present as a single copy, enabling gene inactivation (except those genes on chromosome 8); 2) KBM7 cells are human and of the hematopoietic lineage, increasing the likelihood that any genes we identify could be relevant to the natural context for N-BPs, the bones of human patients (*21*); and 3) it is a different cell line and a different mutagenic approach than that we used with CRISPRi in K562 cells (*19*), which allows us to independently assess those results. Using this haploid approach, we identified, *ATRAID*, a.k.a., *APR3/C2orf28* (*22*), as the gene most significantly enriched for insertions in alendronate resistant cells compared to untreated cells (Fig. 1B; fig. S1, A and B, and table S1). Providing confidence in our screen, we also identified *SLC37A3* as well as *SNTG1*, *PLCL1*, and *EPHB1,* which have been previously connected to N-BP action on bone cells and/or human bone diseases (table S1) (*23-25*).

ATRAID was named because it is a gene whose mRNA expression is strongly induced by the ligand, all-trans retinoic acid (*22*). *ATRAID* is conserved in chordates and contains a signal peptide, Toll-like-receptor leucine rich repeat, EGF-like domain, and a transmembrane domain (Fig. 1C and fig. S1A) (*26, 27*). Importantly, the alendronate resistance phenotype of *ATRAID* deficient cells (ATRAID_GT1 (gene-trap1) and ATRAID_GT2 (gene-trap2)) was reversed by the

re-introduction of wild-type *ATRAID* splice variant 2 (v2) or splice variant 3 (v3) cDNA, which differ in their N-termini (Fig. 1D; fig. S1, A and B). To better understand the level of alendronate resistance in *ATRAID* deficient cells, we varied both cell number and drug concentration in the viability assay. *ATRAID* deficient cells were resistant to alendronate over two to three orders of magnitude of drug concentration or cell number (fig. S1C). Overexpression of full-length *ATRAID* (v2) sensitized cells to alendronate (fig. S1D). Lastly, ATRAID membrane targeting is required for the anti-proliferative effects of alendronate, as *ATRAID* deficient cells complemented with full-length ATRAID (v2) were sensitive to the cytotoxic effects of alendronate, whereas those expressing the membrane truncated form remained resistant (fig. S1E). Taken together, these data establish *ATRAID* as a genetic factor required for the growth inhibitory effects of alendronate.

N-BPs are part of a larger class of compounds known as bisphosphonates (BPs) that contain two phosphate moieties each joined to a carbon atom by a carbon-phosphorus bond (*28*) (Fig. 1E). To determine whether the effects of *ATRAID* deficiency on alendronate resistance were specific to nitrogen-containing bisphosphonates, we tested the effect of several nitrogen-containing and non-nitrogen-containing bisphosphonates on wild-type and mutant *ATRAID* cells. *ATRAID* deficient cells were resistant to the nitrogen-containing bisphosphonates, alendronate and zoledronate, but were as sensitive to the non-nitrogen-containing bisphosphonates, etidronate and tiludronate, as control cells (Fig. 1E).

To determine whether *ATRAID* is required for the reduction in protein prenylation observed upon N-BP treatment, we monitored the prenylation of several proteins, including the heat shock protein DnaJ (Hsp40) homolog HDJ-2, and the Ras family GTPase Rap1a (*29*). Alendronate strongly inhibited prenylation of HDJ-2 and Rap1a in wild-type cells in a dose dependent manner, and had much less of an effect on prenylation of these proteins in *ATRAID*-deficient

cells (Fig. 1F). Furthermore, the inhibitory effect of alendronate on prenylation was rescued when *ATRAID* cDNA variants (v2 and v3) were introduced (fig. S1F). We observed inhibition of prenylation resistance at N-BP doses where we did not see PARP-1 cleavage in *ATRAID* deficient cells, suggesting that *ATRAID* can mediate the effect on prenylation independent of apoptosis (fig. S1F). Thus, these findings suggest *ATRAID* functions as a positive regulator upstream of FDPS.

ATRAID is required for organismal responses to nitrogen-containing bisphosphonates

To determine whether *ATRAID* modulates organismal responses to N-BPs we inactivated *ATRAID* globally in mice (*30*). We confirmed deletion of *ATRAID* exons 3-5 and determined that *ATRAID* homozygous deleted *ATRAID*^{KO} mice (labeled KO, -/-) are viable but their body weight is mildly reduced compared with litter-matched derived, wild-type controls (labeled as WT, +/+) (fig. S2A-C). We confirmed that tail fibroblasts derived from *ATRAID*^{KO} animals are resistant to the cytotoxic effects of alendronate (fig. S2, D and E). Before studying the effects of the N-BPs in the context of *ATRAID* loss, we first characterized the basal role of *ATRAID* in bones. We determined that *ATRAID* mRNA expression was undetectable in the bones of *ATRAID*^{KO} animals and that *ATRAID*^{KO} mice had slightly smaller bones compared with litter-matched derived, wild-type control mice (fig. S2, F and G). To examine the effects of *ATRAID* on bone structure, we performed micro-computed tomography (μCT) analysis (*31*). *ATRAID* deficiency did not significantly decrease either trabecular and cortical structural parameters (fig. S2, H and I; table S2). We measured bone strength using three-point bending tests (*32*). Some measures, such as stiffness (Newtons/millimeter, N/mm) and post-yield displacement (a measure of bone fragility, in millimeters, mm) were decreased by *ATRAID* deficiency, whereas others such, as yield load (the point where bone bending goes from elastic vs. plastic, in Newtons, N), were not significantly altered (fig. S2, J-L; table S2).

Osteoclasts release degradation products from C-terminal telopeptides of type I collagen (CTX-I) from bone into blood (*33*), and levels of CTX-I in serum were not significantly different in wild-type mice compared with *ATRAID*^{KO} mice (fig. S2M; table S2). Histomorphometric measures of osteoclast function including osteoclast surface per bone surface (Oc.S/BS) (*34*), as judged by Tartrate Acid Resistant Phosphatase TRAP staining (*35*), were also not statistically different (fig. S2N; table S2). Consistent with a basal defect in osteoblast function, *ATRAID*^{KO} mice have reduced serum levels of circulating Gla-Osteocalcin (Gla-OC; the activated form of osteocalcin, incorporated in bone matrix (*36*)) and modestly reduced bone formation rate (BFR) as measured by double-labeling (*34*) (fig. S2, O and P; table S2).

To test the effect of alendronate in a model that mimics menopausal bone loss, the most common indication for the N-BPs, we performed ovariectomies (OVX) on adult female mice (Fig. 2A) (*37*). When ovaries are removed from females, the changes in estrogen cause a reduction in bone density triggered by disruption of the balance of osteoblast and osteoclast functions. This loss of bone density can be alleviated by treatment with N-BPs (*38*). The magnitude of trabecular bone loss in WT and *ATRAID* ^{KO} sham mice four weeks after OVX is exemplified in the µCT 3D reconstruction of the femoral proximal metaphysis (Fig. 2B). Consistent with alendronate preventing bone loss (*38*), femoral cortical and trabecular structural parameters, including cortical thickness and area, bone volume/trabecular volume (%) and trabecular thickness, were increased by alendronate treatment of WT OVX mice (Fig. 2, C-F and table S2; see WT OVX +/- alendronate). In contrast, alendronate had blunted effects in *ATRAID* ^{KO} OVX mice (Fig. 2, C-F and table S2; see *ATRAID* ^{KO} OVX +/- alendronate). The same patterns of resistance in *ATRAID*^{KO} mice were observed for bone strength (Fig. 2, G and H). That is, alendronate increased bone strength as judged by stiffness and yield load in wild-type ovariectomized mice, but its effects were significantly blunted in *ATRAID*^{KO} matched

cohorts (Fig. 2, G and H; table S2). Taken together, these results suggest that ATRAID is required for the bone-preserving effects of N-BPs in mice.

ATRAID is required cell-autonomously for N-BP inhibition of osteoclast function

Because N-BPs potentially affect osteoclasts and osteoblasts, we investigated whether ATRAID deficiency would regulate the effects of alendronate in each cell type in our osteoporosis model. Regarding osteoclasts, in wild-type mice both serum and bone histological markers of osteoclast function, CTX-I, and osteoclast surface per bone surface (Oc.S/BS) and osteoclast number per bone surface (N.Oc/BS), respectively, were impaired by alendronate treatment (Fig. 3, A and B; fig. S3A; table S2). In contrast, in *ATRAID*^{KO} mice, alendronate was noticeably less effective on osteoclasts (Fig. 3, A and B; fig. S3A; table S2). That osteoclast number was reduced by N-BPs in wild-type mice is consistent with our cell viability measurements in non-osteoclasts (Fig. 1; fig. S1, S2) and with previous literature (*38*).

To provide insight into the effects of N-BPs on osteoblasts in our osteoporosis model, we measured BFR and mineral apposition rate (MAR) (*34*). Unlike BFR where the bone formation rate is normalized by the amount of labeled bone surface, MAR is the rate of bone formation irrespective of how much of the bone is active (*34*). Alendronate did not affect trabecular MAR or BFR in either wild-type or *ATRAID*^{KO} mice (fig. S3, B and C; table S2).

To determine whether *ATRAID* is required in a cell autonomous manner for the N-BP-dependent effects on osteoclasts, we isolated M-CSF expanded, bone marrow macrophages (BMMs) from both WT and ATRAID^{KO} mice, and differentiated these cells into osteoclasts following a standard protocol (*39*). *ATRAID*^{KO} BMMs differentiated into osteoclasts as well as wild-type cells, irrespective of treatment with alendronate, and BMM-derived *ATRAID*^{KO} osteoclasts were resistant to alendronate-induced apoptosis (Fig. 3, C and D). This suggests

that *ATRAID* is required cell autonomously in osteoclasts for the effects of N-BPs on cell number.

As an independent confirmation of our primary cell experiments, we generated *ATRAID* knockout RAW 264.7 cells and differentiated them to osteoclasts (fig. S3D). RAW 264.7 cells are a robust, well-characterized murine macrophage cell line that can be differentiated to osteoclast-like cells using RANKL (*40*). We treated both RAW 264.7 cells and the RAW 264.7 cells differentiated into osteoclasts with alendronate, and found *ATRAID* deficiency, as expected, conferred resistance to doses that induced apoptosis (Fig. 3E). Alendronate did not affect known markers of osteoclast differentiation in wild-type cells (Fig. 3C). Therefore, to pursue the mechanism of N-BPs on osteoclast function, we focused on prenylation. In alendronate-treated RAW 264.7 and differentiated RAW 264.7 to osteoclast cells, we found *ATRAID*^{KO} cells were resistant to alendronate-induced inhibition of prenylation (Fig. 3F). In total, these findings suggest that *ATRAID* is required for the cell-autonomous effects of N-BPs on osteoclast prenylation.

Genetic factors involved in responses to nitrogen-containing bisphosphonates in patients

We sought an unbiased approach to determine what genes might be relevant in patients treated with N-BPs. We performed exome sequencing of osteoporotic patients who experienced atypical femoral fractures (AFF) when taking N-BPs and compared their DNA with osteoporotic patients who didn't suffer this side effect (Fig. 4A and table S3; see also Materials and Methods for details on how this dataset was generated and analyzed). We also analyzed two published gene expression datasets involving patients who had taken N-BPs: multiple myeloma patients who did or did not suffer osteonecrosis of the jaw (ONJ) when taking N-BPs (*41*); and breast cancer patients with bone marrow disseminated tumor cells (DTC) which reoccurred or the

patient died less than 1000 days vs. greater than 2500 days following initiation of zoledronate treatment (*42*) (Fig. 4A and table S3). In comparing the AFF "hits" – i.e., genes that had rare coding variants in multiple AFF patients but not in controls – with our "hits" from our cell-based alendronate and zoledronate CRISPRi screens (*19*) we identified 165 genes including *ATRAID, FDPS,* and *SLC37A3* (Fig. 4A). When comparing the AFF hits with the ONJ and DTC gene expression studies we identified 68 genes, while the CRISPRi and the two gene expression studies had 137 genes in common (Fig. 4A). Five genes, *ATRAID, ATR, CTC1, MINK1, ZBTB4,* were statistically significant in all datasets (Fig. 4A). We expected decreased *ATRAID* expression (and putatively less N-BP uptake in bone) to be associated with less risk of ONJ and DTC (Fig. 4B and table S3). However, each of the top five genes were differentially expressed in either the ONJ, DTC, or both datasets in the "unexpected" direction based on our loss-of-function results with the N-BPs (table S3) (*19*). This suggests complex relationships of these genes with N-BP outcomes that is worthy of future study. Nevertheless, this data suggests *ATRAID* may be important for N-BP responses in people.

DISCUSSION

This work has focused on the physiological impact of *ATRAID* as a novel positive regulator genetically upstream of *FDPS*. Here we use prenylation as an output of FDPS function. Recently, we linked *FDPS* to DNA synthesis and damage (*43*). Considering each of the five top genes from the patient analysis, *ATRAID*, *ATR, CTC1*, *MINK1*, and *ZBTB4,* are involved in p53 responses – a well-known mediator of DNA damage (Fig. 4A) (*44-48*) – it will be interesting to determine whether these genes mediate their effects on p53 signaling via *FDPS*. The molecular effects of the N-BPs on FDPS require the novel transporter, SLC37A3 (*19*). Interestingly, the SLC37A family member (*49*), *SLC37A2*, is mutated in dogs and gives rise to a bone overgrowth phenotype that resembles the human disease, Caffey syndrome (*50, 51*). This phenotype is particularly interesting because it suggests that natural ligands or drugs that inhibit the SLC37A

family might phenocopy N-BP treatment in increasing bone density. ATRAID binds Nell-1, a secreted protein that promotes bone mineralization in mice and potentiates osteoblast differentiation in an *ATRAID*-dependent manner (*52, 53*). It is also notable that Nell-1 is in pre-clinical testing for the treatment of osteoporosis (*54*). In future studies, it will be interesting to determine whether Nell-1 affects the responses to N-BPs we observe upon manipulating *ATRAID*. There are rare, but serious clinical issues with N-BPs. Therefore, identifying those patients who might experience these consequences when taking N-BPs is of paramount importance. Perhaps utilizing *ATRAID* and/or other factors characterized herein as biomarker(s) might eventually be such a diagnostic strategy.

Materials and Methods

Materials. Reagents were obtained from the following sources: antibodies to Rap1a (SC-1482) from Santa Cruz Biotechnology; anti-HDJ-2/DNAJ Ab-1, Clone: KA2A5.6 (cat.# MS-225-P0), anti-V5 (cat.# R960-25), and GAPDH (14C10) Rabbit mAb (cat.# 2118S) from Fisher Scientific; rabbit polyclonal and monoclonal antibodies to PARP (cat.# 9532) from Cell Signaling Technology; FuGENE 6 (cat.# E2691) and Complete Protease Cocktail (cat.# 11836170001) from Roche; alendronate (cat.# 1012780-200MG), etidronate (cat.# P5248-10MG), tiludronate (cat.# T4580-50MG), Acid Phosphatase Leukocyte (TRAP) kit (cat.# 387A-1KT), SYBR Green JumpStart Taq ReadyMix (cat.# 4309155), calcein (cat.# C0875-5G), FLAG M2 affinity agarose beads (Cat.# M2220), and anti-FLAG antibody (F3165), 3X FLAG peptide (F4799), and alizarin red (cat.# A3882-1G) from Sigma-Aldrich. Zoledronic acid (zoledronate, cat.# M 1875) from Moravek; IMDM Glutatmax, α-MEM, RPMI, SuperScript II Reverse Transcriptase, Platinum Pfx, Platinum Taq DNA Polymerase and inactivated fetal calf serum (IFS) from Invitrogen.

Cell lines and cell culture. KBM7 cell lines were cultured in IMDM with 10% IFS. K562 cell lines were cultured in IMDM or RPMI with 10mM Glutamine with 10% FBS. HEK-293T cells were cultured in DMEM with 10% FBS. RAW264.7 and primary mouse cells were cultured as described below.

Haploid genetic screening. The genetic selection with alendronate was performed on 100 million mutagenized KBM7 cells (*55*). Cells were exposed to 165 μM alendronate and allowed to recover for 4 weeks before harvesting the surviving cells and isolating genomic DNA. Analysis of the screen was performed essentially as described previously (*55*). In brief, the sequences flanking retroviral insertion sites were determined using inverse PCR followed by Illumina sequencing. After mapping these sequences to the human genome, we counted the number of inactivating mutations (i.e., mutations in the sense orientation or present in exon) per individual Refseq-annotated gene as well as the total number of inactivating insertions for all Refseq-annotated genes. For each gene, statistical enrichment was calculated by comparing how often that gene was mutated in the drug-treated population with how often the gene carries an insertion in the untreated control dataset. For each gene, the P-value (corrected for false discovery rate) was calculated using the one-sided Fisher exact test (table S1).

cDNA manipulations and mutagenesis. The cDNAs for *ATRAID* were cloned from a human R4 cell line cDNA library. For expression studies, all cDNAs were amplified by PCR and the products were subcloned into the Sal 1 and Not 1 sites of pRK5 or pMSCV (*56*). The controls, *metap2* and *tubulin*, were previously described (*57*). All constructs were verified by DNA sequencing. To generate the 293T *ATRAID_KO* expressing *ATRAID-FLAG*, using Gibson assembly we cloned the cDNA encoding *ATRAID* with a C-terminal Flag tag into a homologous recombination vector targeting the *AAVS1* locus. We transfected this vector along with pX330 expressing an sgRNA targeting the *AAVS1* locus.

sgRNA manipulations. Genome editing experiments were designed based on an established protocol (*58*). In brief, the sgRNAs for *ATRAID* were cloned using Golden Gate assembly into pSpCas9-BB-2A-GFP (PX438), a kind gift from Feng Zhang (Addgene #48138). All constructs were verified by PCR and DNA sequencing. For the human *ATRAID* locus, one sgRNA targeting exon 3 and another targeting exon 5 were used to act simultaneously and remove part of exon 3, the entire exon 4 and part of exon 5.

Human *ATRAID*:

exon3 sgRNA_1: GCCTGATGAAAGTTTGGACC

exon3 sgRNA_2: CCCTGGTCCAAACTTTCATC

exon5 sgRNA_1: GTCCTGGAGGAATTAATGCC

exon5 sgRNA_2: GTCCTGGAGGAATTAATGCC

Mouse *ATRAID*:

GGATACATCGAAGCTAATGC

For generating *ATRAID* knockouts in RAW 264.7 cells, cells were transfected with PX438 carrying the above sgRNA. Mutation was confirmed by PCR and sequencing.

Cell viability assays. Wild-type or mutant cells were seeded at 20,000 cells per well in a 96-well tissue culture plate and treated with indicated concentrations of compound or left untreated. 48 or 72 hours after treatment the cell viability was measured using a Cell-titer Glo colorimetric assay (Promega) according to manufacturer's protocol. Viability is plotted as percentage viability compared to untreated control.

For assays of apoptosis, cells were plated in 6-well dishes and exposed to alendronate for 48

hours. AnnexinV positive cells were quantified using flow cytometry with the Dead Cell Apoptosis Kit with AnnexinV Alexa Fluor (488) and PI (Thermo Fisher Scientific #V13241) following the manufacturer's instructions.

Protein analysis. All cells unless otherwise stated were rinsed twice with ice-cold PBS and lysed with Triton-X 100 or NP-40 containing lysis buffer (40 mM HEPES [pH 7.4], 2 mM EDTA, 150 mM NaCl, 50 mM NaF, 1% Triton-X 100 or 1% NP-40, and one tablet of EDTA-free protease inhibitors [Roche] per 25 ml or Halt protease-phosphatase inhibitor (#78442 ThermoFisher Scientific)). Lysate is incubated at 4 centigrade for 15-30min with constant inversion. The soluble fractions of cell lysates were isolated by centrifugation at 13,000 rpm for 10 min in a microcentrifuge. Lysate protein concentrations were normalized by Bradford assay (Bio-Rad). Proteins were then denatured by the addition of sample buffer and by boiling for 5 minutes, resolved using 4%-20% or 6% (for HDJ-2) SDS-PAGE (Invitrogen), and analyzed by immunoblotting for the indicated proteins. Immunoblotting was performed as follows: nitrocellulose membranes were blocked at room temperature (RT) with 5% non-fat milk for 45min. Membranes were then incubated overnight at 4°C with desired primary antibodies dissolved in 5% milk. Membranes were then washed 3 times in TBST, each wash lasting 5min. Membranes were then incubated at RT with desired secondary antibodies at 1:2000 in 5% milk for 45min. HRP-conjugated or fluorescent secondary antibodies (Santa Cruz Biotechnology or Thermo Fisher, respectively) were used for detection. Membranes were then washed 3 times in TBST, each wash lasting 5min. Signal from membranes using HRP-conjugated secondary antibodies were captured using a camera and those using fluorescent secondary antibodies were imaged on a GE Typhoon Trio imager. The small GTPase Rap1A protein prenylation can be detected by Western blot analysis using an antibody that specifically binds to its unprenylated form (*59, 60*) (Santa Cruz, SC-1482).

RAW 264.7 differentiation. RAW 264.7 cells were maintained in DMEM + 10% FBS + 1X penicillin/streptomycin. Differentiation of RAW cells to osteoclasts was achieved following the protocol of Collin-Osdoby et al. (*40*) where cells were treated with 35ng/ml RANKL (R&D Systems) for 6 days. For experiments with alendronate, the drug was added at the indicated concentrations 48 hours prior to collection.

Primary bone marrow isolation and osteoclast differentiation. Primary bone marrow was isolated from the femurs, tibiae, and spine of wildtype and *ATRAID*^{KO} mice, enriched to macrophages and differentiated to osteoclasts following the protocol of Tevlin et al. (*39*). Where indicated, cells were treated with the indicated concentration of alendronate 48 hours before collection.

Gene expression analysis. Total RNA was isolated and reverse-transcription was performed from cells or tissues in the indicated conditions. The resulting cDNA was diluted in DNase-free water (1:20) followed by quantification by real-time PCR. mRNA transcript levels were measured using Applied Biosystems 7900HT Sequence Detection System v2.3 software. All Data are expressed as the ratio between the expression of target gene to the housekeeping genes 36B4 and/or GAPDH. Each treated sample was normalized to the level of the controls in the same cell type.

Human Primer sequences (for clarity, denoted with prefix: “h” for human):

hATRAID exon1-F’ – GGATGGAGGGGCCCGAGTTTCTG

hATRAID exon2-R’ – CCCAAGATGGTGCCCTTCTGATTC

hATRAID exon6-F’ – CCATGGATACAAGTGTATGCGCC

hATRAID exon 7-R’ – TCATGAAGTCTTGGCTTTTCGGC

Mouse Primer sequences (for clarity, denoted with prefix: “m” for mouse):

mATRAID exon3-F’ – GATCTTCAGAACTGTTCCCTGAAG

mATRAID exon4-R’ – GCTGAGTAAACCCACGGAAGGTG

mATRAID exon5-F’ – CTTCTTTCAAGGACAAGCAGATTTG

mATRAID exon 7-R’ – GAATCCCAAAGAACATAAGCAGTG

mACTB- F’- TGTCGAGTCGCGTCCA

mACTB- R’ – ATGCCGGAGCCGTTGTC

mRPLP0- F’ – TGCTCGACATCACAGAGCAG

mRPLP0- R’ – ACGCGCTTGTACCCATTGAT

mRANK – F’ – GCAGCTCAACAAGGATACGG

mRANK – R’- TAGCTTTCCAAGGAGGGTGC

mTRAP –F’ – AAGAGATCGCCAGAACCGTG

mTRAP – R’ – CGTCCTCAAAGGTCTCCTGG

mCTSK – F’ – CCTTCCAATACGTGCAGCAG

mCTSK- R’ – CATTTAGCTGCCTTTGCCGT

Generation and genotyping of ATRAID KO mice*.* Chimeric mice were obtained by microinjection of the correctly targeted *ATRAID* EUCOMM ES clones (HEPD0577_2_D01 and HEPD0577_2_E01) (*61, 62*) into BALB/C blastocysts and crossed with C57BL/6 mice to obtain

offspring with germline transmission. Heterozygous mice for the floxed *ATRAID* allele (*ATRAID*$^{loxP/+}$), were crossed to C57BL/6 mice expressing the Cre-recombinase transgene from the full-body CMV promoter (*63*). Mice analyzed in this study were 100% C57BL/6.

All experiments involving mice were performed with protocols approved by the Harvard and Washington University Animal Studies Committees. We confirm that we have complied with all relevant ethical regulations. All mice were housed under a 12-hour light cycle and fed standard chow diet ad libitum.

PCR genotyping of all WT and *ATRAID* deficient mice were performed with primers that detect the following:

1) This generates a 140bp product and indicates the presence of the transgene.

Transgene (92 upstream) F' CAGCCATATCACATCTGTAGAG

Transgene (92 upstream) R' GAGTTTGGACAAACCACAACTAG

2) This indicates recombination and is detectable in mice also expressing CRE

Del F' CTGCATTCTAGTTGTGGTTTGTCC

Del R' CAGGAGGTAGTGCAAGCCTTTG

3) Wild-type *ATRAID* primers spanning *ATRAID* exons 3 and 4. This PCR product is not detectable in homozygous null animals.

Exon 3/4 F' CAGAACTGTTCCCTGAAGGATCCTGGTC

Exon 3/4 R' GTACACACTGTTAGCGCTCTGTTTGC

4) These generic CRE primers give a ~100bp product indicates the presence of the CRE transgene.

CRE F' GCG GTC TGG CAG TAA AAA CTA TC

CRE R' GTG AAA CAG CAT TGC TGT CAC TT

Serum ELISA assays. Cardiac puncture blood of mice of the indicated ages was obtained and centrifuged at low speed at 4°C for 15 min, and serum was isolated. Gla-Osteocalcin (Mouse Gla-Osteocalcin High Sensitive EIA Kit from Clontech, cat.# MK127) and C-terminus cross-linked telopeptides of type I collagen CTX-I (RatLaps EIA Kit from Immunodiagnosticsystems Inc., Bolden, UK, AC-06F1) were quantified following the manufacturer instructions.

Animal procedures. Age and sex matched mice were randomly assigned to treatment groups within each genotype. All animal experiments were replicated two to four times spanning independent days to ensure reproducibility.

Ovariectomy or sham operations were performed on 3.5-month-old females as detailed previously (*64*). Briefly, the ovaries were exposed through an abdominal approach and either resected after clipping the blood vessels or left in place (sham operation). The muscle and skin of the abdomen were sutured. Mice were given an intraperitoneal injection of buprenex immediately after surgery and then every twelve hours for 48 hours post-surgery. Immediately preceding OVX, vehicle (phosphate buffered saline) or 100 µg/kg alendronate (both provided by Sigma) was injected intra-peritoneally every week for 4 weeks. These doses were chosen based on the anti-resorptive activity of alendronate in different species (*65, 66*).

Bone microstructure. A high-resolution desktop micro-tomographic imaging system (µCT40, Scanco Medical AG, Bruttisellen, Switzerland) was used to assess cortical and trabecular bone microarchitecture and morphology in the femoral mid-diaphysis and distal metaphysis, respectively. Scans were acquired using a 10 μm^3 isotropic voxel size, 70 kVP peak x-ray tube potential, 114 mAs x-ray intensity, 200 ms integration time, and were subjected to Gaussian filtration and segmentation. Regions of interest (ROIs) were selected 50 slices above and below the femoral longitudinal midpoint or 100 slices above the growth plate of the distal femur to

evaluate the cortical and trabecular compartment, respectively. Image acquisition and analysis adhered to the JBMR guidelines for the use of μCT for the assessment of bone microarchitecture in rodents (*31*).

Bone biomechanics. Mechanical testing in a 3-point bending to failure was conducted on femora after μCT. Briefly, hydrated femora were stabilized over supports 7mm apart and a loading force was applied in the anteroposterior direction midway between the supports (Instron, Norwood, MA, USA). Test curves were analyzed to determine ultimate force to failure and stiffness as described previously (*32, 67*).

Bone histomorphometry. To label mineralizing fronts, mice were injected intraperitoneally with calcein (15 mg/kg i.p., Sigma-Aldrich) and alizarin red (30 mg/kg; Sigma) were intraperitoneally injected 7 and 2 days, respectively, before euthanasia. Bone was fixed in 10%(vol/vol) neutral buffered formalin for 24 h, processed through a series of graded alcohols, and decalcified. Decalcified vertebrae or femurs were embedded in paraffin and 2-4 h, processed through a series of graded alcohols, and Tartrate resistant acid phosphatase (TRAP) stain was performed. Undecalcified femora were embedded in methyl methacrylate and the whole bone were cut and stained for TRAP or analyzed for calcein and alizarin red fluorescence. Quantitative histomorphometry was performed using a commercial software (OSTEO II, Bioquant, Nashville, TN, USA), and standard parameters of bone remodeling were determined as detailed elsewhere (*68*).

Statistics analysis. Unless otherwise specified, group means were compared by one-tailed Student t-test for unpaired samples. Data on repeated measures were analyzed by ANOVA, followed by a post-hoc multiple Holm–Sidak method t-test. All data are expressed as the mean ± s.d with numbers of samples indicated in figure legends. *P* values are indicated in each figure

legend, and values less than 0.05 were considered significant. All code used to generate statistics and correlations for this project can be found at https://github.com/tim-peterson/ATRAID.

Transcriptional profiling analysis. The multiple myeloma, osteonecrosis of the jaw (ONJ) microarray gene expression was performed as previously described (*41*) using the Affymetrix U133 Plus 2.0 array platform (Affymetrix, Santa Clara, CA, USA) on total RNA isolated from peripheral blood mononuclear cells (GEO accession #: GSE7116). 21 multiple myeloma patients with a history of N-BP use were included in the study. 11 patients (52.4%) reported to have ONJ. The breast cancer bone marrow micrometastases (a.k.a., DTC) microarray gene expression data was generated as previously described (*42*) and also used the Affymetrix U133 Plus 2.0 array platform. DTC profiling was performed on tumor biopsies of 81 patients (GEO accession #: GSE71258). 54 breast cancer patients treated with zometa (zoledronate) were included in the study. N-BPs directly inhibit tumor growth and angiogenesis (*69, 70*). 14 patients (25.9%) eventually died and 40 patients (74.1%) survived. Her-2 negative patients were divided into two categories following randomization to the zoledronate arm: those that who had DTC reoccurrences or lived less than 1000 days and those who lived at least 2500 days.

Quantile normalization was used for all differential expression analysis, and all the normalization procedures were performed using function normalizeQuantiles in the R Bioconductor package limma (*71*). Gene expression data was filtered using function filterfun in the R Bioconductor package genefilter (*72*). Probes with expression values over 5 in less than 25% of the samples were removed. Comparison between groups were estimated using an empirical Bayes method (*73*), and variances across all genes were used to estimate the variance of each gene. Raw p-values were calculated from a moderate t-test, and false discovery rate (FDR) adjusted p-values

were obtained based on Benjamini and Hochberg's methods for multiple testing. Log_2 fold changes between the experimental conditions were calculated for each gene as well.

Affy probe IDs were transformed into gene symbols based on the R Bioconductor package, hgu133plus2.db (*74*). In Fig. 4A, differentially regulated genes for the -/+ONJ patients were identified by having adjusted p-values smaller than 0.05, while potential differentially-regulated genes for the <1000 vs. >2500 days with breast cancer patients with disseminated tumor cells (DTC) were identified by having raw p-value smaller than 0.05. For the ONJ dataset, 1992 genes were significant. For the DTC dataset, 1854 genes were significant.

Exome sequencing analysis. Exome sequencing data was generated from blood leukocyte DNA for 28 bisphosphonate treated osteoporosis cases with atypical femoral fractures (AFF) and 11 bisphosphonate treated osteoporosis cases without atypical femoral fractures. Exome capture was performed using Agilent All-exome capture kits. Sequencing was performed using paired-end Illumina sequencing. Alignment was performed using the Burrows-Wheeler Aligner (BWA) and variants called using SAMTOOLS. Variant positions were processed excluding those with call rates <0.95 or Hardy-Weinberg equilibrium P-values < 10^{-5}. Genotypes were filtered excluding those with read depth <8x or genotype quality (GQ) < 20. The vcf file was annotated using Seattleseq: http://snp.gs.washington.edu/SeattleSeqAnnotation151/. Genes with multiple variants with non-Finnish European (NFE) allele frequencies less than 0.05 only in cases were considered. From dbSNP, https://www.ncbi.nlm.nih.gov/SNP/ : For the *ATRAID* gene, the D5G variant is found on chromosome 2 position: 27212382 - rs1275533. The G32R variant is found on chromosome 2 position: 27212297 - rs11556163.

The ethnic breakdown of the AFF cases is: 25/28 European American (EA), 3/28 Asian American (AA), 0/28 African American. The ethnic breakdown of the controls is 8/11 European

American and 3/11 unknown. For *ATRAID*, the D5G variant is present in 2 out of 28 AFF patients. Though this allele wasn't detected in the 11 control samples, it is present in a population of European Americans (EA) that is representative of the study population at a prevalence of 0.0139 and in Asian Americans (AA) at a prevalence of 0.002. Therefore, the D5G allele is (2/28) / (0.0139 * 25/28 + 0.002 * 3/28) = 5.66X enriched in cases compared to a representative population to that of the cases. A simple binomial test, binom.test(), was used to calculate the p-value for each variant. For the D5G allele, p-value = 0.04851. For the G32R *ATRAID* allele the enrichment is: (2/28) / (0.0149 * 25/28 + 0.002 * 3/28) = 5.28; p-value = 0.05477.

Supplementary Materials

Fig. S1, related to Fig. 1. ATRAID is required for molecular responses to N-BPs.

Fig. S2, related to Fig. 2. ATRAID is required for organismal responses to N-BPs.

Fig. S3, related to Fig. 3. ATRAID is required cell-autonomously for N-BP inhibition of osteoclast function.

Table S1, related to Fig. 1 and fig. S1. Haploid genomic screen raw data for alendronate.

Table S2, related to Fig. 2 and fig. S2. Statistics for animal studies.

Table S3, related to Fig. 4. Gene expression, sequencing, and growth phenotype data for ONJ, DTC, AFF, and CRISPRi studies.

References and Notes:

1. J. J. Carey, L. Palomo, Bisphosphonates and osteonecrosis of the jaw: innocent association or significant risk? *Cleveland Clinic journal of medicine* **75**, 871-879 (2008)
2. J. P. van den Bergh, T. A. van Geel, P. P. Geusens, Osteoporosis, frailty and fracture: implications for case finding and therapy. *Nat Rev Rheumatol* **8**, 163-172 (2012)
3. R. E. Coleman, E. V. McCloskey, Bisphosphonates in oncology. *Bone* **49**, 71-76 (2011)
4. D. M. Black, C. J. Rosen, Clinical Practice. Postmenopausal Osteoporosis. *N Engl J Med* **374**, 254-262 (2016)
5. N. B. Watts, D. L. Diab, Long-term use of bisphosphonates in osteoporosis. *J Clin Endocrinol Metab* **95**, 1555-1565 (2010)

6. Y. Bi *et al.*, Bisphosphonates cause osteonecrosis of the jaw-like disease in mice. *Am J Pathol* **177**, 280-290 (2010).2893671
7. S. Khosla *et al.*, Addressing the Crisis in the Treatment of Osteoporosis: A Path Forward. *J Bone Miner Res*, (2016)
8. S. P. Luckman *et al.*, Nitrogen-containing bisphosphonates inhibit the mevalonate pathway and prevent post-translational prenylation of GTP-binding proteins, including Ras. *J Bone Miner Res* **13**, 581-589 (1998)
9. E. van Beek, E. Pieterman, L. Cohen, C. Lowik, S. Papapoulos, Nitrogen-containing bisphosphonates inhibit isopentenyl pyrophosphate isomerase/farnesyl pyrophosphate synthase activity with relative potencies corresponding to their antiresorptive potencies in vitro and in vivo. *Biochem Biophys Res Commun* **255**, 491-494 (1999)
10. J. D. Bergstrom, R. G. Bostedor, P. J. Masarachia, A. A. Reszka, G. Rodan, Alendronate is a specific, nanomolar inhibitor of farnesyl diphosphate synthase. *Arch Biochem Biophys* **373**, 231-241 (2000)
11. M. J. Favus, Bisphosphonates for osteoporosis. *N Engl J Med* **363**, 2027-2035 (2010)
12. C. J. Rosen, Clinical practice. Postmenopausal osteoporosis. *N Engl J Med* **353**, 595-603 (2005)
13. R. Coleman, The use of bisphosphonates in cancer treatment. *Ann N Y Acad Sci* **1218**, 3-14 (2011)
14. S. Jha, Z. Wang, N. Laucis, T. Bhattacharyya, Trends in Media Reports, Oral Bisphosphonate Prescriptions, and Hip Fractures 1996-2012: An Ecological Analysis. *J Bone Miner Res* **30**, 2179-2187 (2015)
15. A. A. Reszka, G. A. Rodan, Nitrogen-containing bisphosphonate mechanism of action. *Mini Rev Med Chem* **4**, 711-719 (2004)
16. V. Breuil *et al.*, Human osteoclast formation and activity in vitro: effects of alendronate. *J Bone Miner Res* **13**, 1721-1729 (1998)
17. Z. Zimolo, G. Wesolowski, G. A. Rodan, Acid extrusion is induced by osteoclast attachment to bone. Inhibition by alendronate and calcitonin. *J Clin Invest* **96**, 2277-2283 (1995).185878
18. D. E. Hughes *et al.*, Bisphosphonates promote apoptosis in murine osteoclasts in vitro and in vivo. *J Bone Miner Res* **10**, 1478-1487 (1995)
19. Z. Yu *et al.*, Identification of a transporter complex responsible for the cytosolic entry of nitrogen-containing-bisphosphonates. *Elife* **7**, (2018)
20. J. E. Carette *et al.*, Haploid genetic screens in human cells identify host factors used by pathogens. *Science* **326**, 1231-1235 (2009)
21. A. J. Roelofs, K. Thompson, F. H. Ebetino, M. J. Rogers, F. P. Coxon, Bisphosphonates: molecular mechanisms of action and effects on bone cells, monocytes and macrophages. *Curr Pharm Des* **16**, 2950-2960 (2010)
22. F. Zhu *et al.*, Improved PCR-based subtractive hybridization strategy for cloning differentially expressed genes. *Biotechniques* **29**, 310-313 (2000)
23. S. Bashiardes *et al.*, SNTG1, the gene encoding gamma1-syntrophin: a candidate gene for idiopathic scoliosis. *Hum Genet* **115**, 81-89 (2004)
24. Y. Z. Liu *et al.*, Identification of PLCL1 gene for hip bone size variation in females in a genome-wide association study. *PLoS One* **3**, e3160 (2008).PMC2522269
25. E. Shimizu, J. Tamasi, N. C. Partridge, Alendronate affects osteoblast functions by crosstalk through EphrinB1-EphB. *J Dent Res* **91**, 268-274 (2012).PMC3275334
26. G. Yang *et al.*, Identification of the distinct promoters for the two transcripts of apoptosis related protein 3 and their transcriptional regulation by NFAT and NFkappaB. *Mol Cell Biochem* **302**, 187-194 (2007)
27. Phyre2, http://www.sbg.bio.ic.ac.uk/phyre2/html/page.cgi?id=index. *Protein Homology/analogY Recognition Engine V 2.0*, (website)

28. R. G. Russell, Bisphosphonates: the first 40 years. *Bone* **49**, 2-19 (2011)
29. K. Thompson, M. J. Rogers, F. P. Coxon, J. C. Crockett, Cytosolic entry of bisphosphonate drugs requires acidification of vesicles after fluid-phase endocytosis. *Mol Pharmacol* **69**, 1624-1632 (2006)
30. W. C. Skarnes *et al.*, A conditional knockout resource for the genome-wide study of mouse gene function. *Nature* **474**, 337-342 (2011).3572410
31. M. L. Bouxsein *et al.*, Guidelines for assessment of bone microstructure in rodents using micro-computed tomography. *J Bone Miner Res* **25**, 1468-1486 (2010)
32. http://www.musculoskeletalcore.wustl.edu/mm/files/Understanding 3pt Bending outcomes.pdf.
33. C. Rosenquist *et al.*, Serum CrossLaps One Step ELISA. First application of monoclonal antibodies for measurement in serum of bone-related degradation products from C-terminal telopeptides of type I collagen. *Clin Chem* **44**, 2281-2289 (1998)
34. D. W. Dempster *et al.*, Standardized nomenclature, symbols, and units for bone histomorphometry: a 2012 update of the report of the ASBMR Histomorphometry Nomenclature Committee. *J Bone Miner Res* **28**, 2-17 (2013).PMC3672237
35. P. Ballanti *et al.*, Tartrate-resistant acid phosphate activity as osteoclastic marker: sensitivity of cytochemical assessment and serum assay in comparison with standardized osteoclast histomorphometry. *Osteoporos Int* **7**, 39-43 (1997)
36. M. Ferron *et al.*, Insulin signaling in osteoblasts integrates bone remodeling and energy metabolism. *Cell* **142**, 296-308 (2010).2910411
37. H. A. Fleisch, Bisphosphonates: preclinical aspects and use in osteoporosis. *Ann Med* **29**, 55-62 (1997)
38. M. P. Watkins *et al.*, Bisphosphonates improve trabecular bone mass and normalize cortical thickness in ovariectomized, osteoblast connexin43 deficient mice. *Bone* **51**, 787-794 (2012).PMC3432742
39. R. Tevlin *et al.*, Osteoclast derivation from mouse bone marrow. *J Vis Exp*, e52056 (2014).PMC4353410
40. P. Collin-Osdoby, P. Osdoby, RANKL-mediated osteoclast formation from murine RAW 264.7 cells. *Methods Mol Biol* **816**, 187-202 (2012)
41. N. Raje *et al.*, Clinical, radiographic, and biochemical characterization of multiple myeloma patients with osteonecrosis of the jaw. *Clin Cancer Res* **14**, 2387-2395 (2008)
42. J. Xiang *et al.*, CXCR4 Protein Epitope Mimetic Antagonist POL5551 Disrupts Metastasis and Enhances Chemotherapy Effect in Triple-Negative Breast Cancer. *Mol Cancer Ther* **14**, 2473-2485 (2015).PMC4784694
43. M. A. Horlbeck *et al.*, Mapping the Genetic Landscape of Human Cells. *Cell*, (2018)
44. S. Han, Q. Lu, N. Wang, Apr3 accelerates the senescence of human retinal pigment epithelial cells. *Mol Med Rep* **13**, 3121-3126 (2016)
45. P. Gu *et al.*, CTC1 deletion results in defective telomere replication, leading to catastrophic telomere loss and stem cell exhaustion. *EMBO J* **31**, 2309-2321 (2012).PMC3364752
46. T. A. Lantto *et al.*, Cellular Stress and p53-Associated Apoptosis by Juniperus communis L. Berry Extract Treatment in the Human SH-SY5Y Neuroblastoma Cells. *Int J Mol Sci* **17**, (2016).PMC4964488
47. E. Lecona, O. Fernandez-Capetillo, Targeting ATR in cancer. *Nat Rev Cancer*, (2018)
48. D. Yamada *et al.*, The human protein kinase HIPK2 phosphorylates and downregulates the methyl-binding transcription factor ZBTB4. *Oncogene* **28**, 2535-2544 (2009)
49. J. Y. Chou, B. C. Mansfield, The SLC37 family of sugar-phosphate/phosphate exchangers. *Curr Top Membr* **73**, 357-382 (2014).PMC4180117

50. M. K. Hytonen *et al.*, Molecular Characterization of Three Canine Models of Human Rare Bone Diseases: Caffey, van den Ende-Gupta, and Raine Syndromes. *PLoS Genet* **12**, e1006037 (2016).PMC4871343
51. A. Guerin, L. Dupuis, R. Mendoza-Londono, in *GeneReviews((R)),* M. P. Adam *et al.*, Eds. (Seattle (WA), 1993).
52. X. Zou *et al.*, NELL-1 binds to APR3 affecting human osteoblast proliferation and differentiation. *FEBS Lett* **585**, 2410-2418 (2011)
53. J. Desai *et al.*, Nell1-deficient mice have reduced expression of extracellular matrix proteins causing cranial and vertebral defects. *Hum Mol Genet* **15**, 1329-1341 (2006)
54. A. W. James *et al.*, NELL-1 in the treatment of osteoporotic bone loss. *Nat Commun* **6**, 7362 (2015).PMC4557288
55. J. E. Carette *et al.*, Global gene disruption in human cells to assign genes to phenotypes by deep sequencing. *Nat Biotechnol* **29**, 542-546 (2011).PMC3111863
56. T. R. Peterson *et al.*, mTOR complex 1 regulates lipin 1 localization to control the SREBP pathway. *Cell* **146**, 408-420 (2011).PMC3336367
57. T. R. Peterson *et al.*, DEPTOR is an mTOR inhibitor frequently overexpressed in multiple myeloma cells and required for their survival. *Cell* **137**, 873-886 (2009).PMC2758791
58. F. A. Ran *et al.*, Genome engineering using the CRISPR-Cas9 system. *Nat Protoc* **8**, 2281-2308 (2013).PMC3969860
59. F. P. Coxon *et al.*, Protein geranylgeranylation is required for osteoclast formation, function, and survival: inhibition by bisphosphonates and GGTI-298. *J Bone Miner Res* **15**, 1467-1476 (2000)
60. J. C. Frith, J. Monkkonen, S. Auriola, H. Monkkonen, M. J. Rogers, The molecular mechanism of action of the antiresorptive and antiinflammatory drug clodronate: evidence for the formation in vivo of a metabolite that inhibits bone resorption and causes osteoclast and macrophage apoptosis. *Arthritis and rheumatism* **44**, 2201-2210 (2001)
61. R. Kuhn, R. M. Torres, Cre/loxP recombination system and gene targeting. *Methods Mol Biol* **180**, 175-204 (2002)
62. http://www.mousephenotype.org/data/alleles/MGI:1918918/tm1a%2528EUCOMM%2529Hmgu?
63. F. Schwenk, U. Baron, K. Rajewsky, A cre-transgenic mouse strain for the ubiquitous deletion of loxP-flanked gene segments including deletion in germ cells. *Nucleic Acids Res* **23**, 5080-5081 (1995).307516
64. C. F. Lai *et al.*, Accentuated ovariectomy-induced bone loss and altered osteogenesis in heterozygous N-cadherin null mice. *J Bone Miner Res* **21**, 1897-1906 (2006)
65. R. K. Fuchs, R. J. Phipps, D. B. Burr, Recovery of trabecular and cortical bone turnover after discontinuation of risedronate and alendronate therapy in ovariectomized rats. *J Bone Miner Res* **23**, 1689-1697 (2008).2684160
66. M. R. Allen, K. Iwata, R. Phipps, D. B. Burr, Alterations in canine vertebral bone turnover, microdamage accumulation, and biomechanical properties following 1-year treatment with clinical treatment doses of risedronate or alendronate. *Bone* **39**, 872-879 (2006)
67. M. D. Willinghamm *et al.*, Age-related changes in bone structure and strength in female and male BALB/c mice. *Calcif Tissue Int* **86**, 470-483 (2010).PMC2895262
68. S. K. Grimston *et al.*, Connexin43 deficiency reduces the sensitivity of cortical bone to the effects of muscle paralysis. *J Bone Miner Res* **26**, 2151-2160 (2011).PMC3306012
69. T. A. Guise, Antitumor effects of bisphosphonates: promising preclinical evidence. *Cancer Treat Rev* **34 Suppl 1**, S19-24 (2008)

70. R. Aft *et al.*, Effect of zoledronic acid on disseminated tumour cells in women with locally advanced breast cancer: an open label, randomised, phase 2 trial. *Lancet Oncol* **11**, 421-428 (2010).PMC3792651
71. B. M. Bolstad, R. A. Irizarry, M. Astrand, T. P. Speed, A comparison of normalization methods for high density oligonucleotide array data based on variance and bias. *Bioinformatics* **19**, 185-193 (2003)
72. C. V. Gentleman R, Huber W and Hahne F (2017).
73. G. K. Smyth, Linear models and empirical bayes methods for assessing differential expression in microarray experiments. *Stat Appl Genet Mol Biol* **3**, Article3 (2004)
74. M. Carlson. (2016).

Acknowledgements: We thank members of the Peterson and Erin O'Shea laboratories for helpful discussions, especially Chris Chow and Kevin Li (Peterson); and A. R. Subramaniam, Christopher Chidley, and Anna Puszynska for illustrations (O'Shea). We thank Mary Bouxsein and Daniel Brooks (Beth Israel Deaconess Medical Center), and Dan Lieb and Matt Silva (Washington University School of Medicine) for bone structure and function analysis. We thank Kenichi Nagano and Roland Baron (Harvard School of Dental Medicine), Yoshiko Iwamoto (Massachusetts General Hospital) and Deb Novack, Gary London, and Crystal Idleburg for histology, histomorphometry, and imaging (Washington University School of Medicine).

Funding: This work was supported by grants from the NIH (CA103866 and AI047389 to D.M.S., HD070394 to B.L.) and Department of Defense (W81XWH-07-0448 to D.M.S.); awards from the W.M. Keck Foundation and the LAM (lymphangioleiomyomatosis) Foundation to D.M.S.; Rolanette and Berdon Lawrence Bone Disease Program of Texas and BCM Center for Skeletal Medicine and Biology and NIDDK training grant 5T32DK060445-10 to A.R.; fellowships from the Jane Coffin Childs Foundation, NIH/NIA K99/R00 (K99AG047255-01/R00AG047255-04), NIH/NIAMS R01 AR073017-01A1, and NIH/NIAMS P30 AR057235 to T.R.P. D.M.S. is an investigator of the Howard Hughes Medical Institute. **Author Contributions:** T.R.P. and L.E.S. designed the study. J.P., A.R., and Z.Y. performed viability assays. S.K. and L.E.S. performed immunoblots. Y.B., B.H.L, D.T.B. and N.S. conducted analysis of both basal and OVX mouse studies. C.L. performed statistical analysis for the patient gene expression and mouse studies.

S.M., J.C.B., M.M., M.S., M.H., S.D., V.N.B., R.C., M.J.G., C.M.M., W.M.R., C.A.G., and K.D. performed the exome sequencing on the atypical fracture patients. G.H. and C.C.G. performed statistical analysis for the atypical fracture patients. M.V., K.B., J.E.C., T.R.B., D.M.S., and J.L. performed and/or provided assistance with the cell-based, genomic screening. T.R.P., J.P., and L.E.S. wrote the paper. **Competing Interests:** ATRAID, SNTG1, EPHB1, and PLCL1, the genes identified here, are part of a Whitehead–Harvard patent on which T.R.P., T.R.B., and D.M.S. are inventors. Shared reagents are subject to a materials transfer agreement. **Data and materials availability:** All data that supports the findings is available in the Figures, supplemental figures and tables.

Figures:

Fig. 1. *ATRAID* is required for molecular responses to nitrogen-containing bisphosphonates. (A) Schematic of haploid mutagenesis screening pipeline. Sequencing-based identification of gene-trap insertion sites in alendronate-resistant human haploid KBM7 cells. Genomic DNA for sequencing was obtained from mutagenized KBM7 cells grown for four weeks post-treatment with 165 μM alendronate. **(B)** Sequencing-based identification of gene-trap insertion sites in alendronate-resistant cells. N=number of unique insertions within the stated gene locus. False discovery rate corrected (FDR) p-values for *ATRAID*=7.02×10^{-45}, *PLCL1*=1.02×10^{-04}, *EPHB1*=2.05×10^{-04}, *SNTG1*= 1.84×10^{-03}. P-values represent enrichment in alendronate-treated versus vehicle treated cells. The red dotted line indicates the genes with a FDR p-value of < 0.05. 185 genes in this screen that met that criteria. **(C)** Schematic representation of structural features of human ATRAID protein and its mouse and frog orthologues. **(D)** Cell viability in wild-type control and *ATRAID*-deficient cells exogenously expressing or not expressing *ATRAID* cDNA. Cells were treated with 60 μM alendronate and analyzed for cell viability. Cell viability was determined by measuring cellular ATP levels and is expressed as a ratio of that compared with untreated cells. Error bars indicate the standard

deviation for n=4 (biological replicates). N.S., not significant; * indicates $p<0.05$. v2, variant 2 (NM_080592.3); v3, variant 3 (NM_001170795.1) of the *ATRAID* gene, respectively. **(E)** Chemical structures for nitrogen-containing bisphosphonates (N-BPs) or non-nitrogen-containing bisphosphonates (BP) used in (E) are shown. KBM7 cell viability in *ATRAID*-deficient (ATRAID_GT1 and ATRAID_GT2) and control (wild-type) KBM7 cells upon treatment with nitrogen-containing bisphosphonates (N-BPs) or non-nitrogen-containing bisphosphonates (BP). All cells were treated with the indicated concentration of the indicated N-BP (alendronate, zoledronic acid), BP (etidronate, tiludronate) for 72 hours. Cell viability was determined by measuring cellular ATP levels and is expressed as a ratio of that compared with untreated cells. All measurements were performed in quadruplicate (biological replicates). * indicates $p<0.05$, unpaired *t*-test. **(F)** Alendronate induced inhibition of protein prenylation requires *ATRAID*. *ATRAID*-deficient and *ATRAID* V3-reconstituted HEK-293T cells were treated with the indicated dose of alendronate for 24 hours then lysed and analyzed by immunoblotting for the indicated proteins. Equal amounts of protein were loaded in each lane. This experiment was repeated three times (biological replicates) and was consistent all three times. * indicates non-specific band.

Fig. 2. ATRAID is required for organismal responses to nitrogen-containing bisphosphonates. (A) Schematic of menopausal bone loss model – bilateral ovariectomy (OVX). Saline or 100 μg/kg/week alendronate was administered concurrent with OVX or a sham procedure. After four weeks, mice were euthanized and bones and serum were extracted and analyzed. **(B)** Representative μCT reconstructions of femoral trabecular bone from 4-month-old litter-matched derived, wild-type, *ATRAID* WT (+/+), and KO (-/-), female mice that were either ovariectomized (OVX) or sham operated (Sham), treated with either vehicle (saline) (+OVX), or alendronate (+OVX+ALN) for four weeks. **(C-F)** Ovariectomized *ATRAID*$^{-/-}$ mice have impaired bone microstructural responses to alendronate. Femur cortical (C, D) and trabeculae (E, F)

regions were analyzed by μCT. Each circle represents an individual animal. Circles offset to the right represent unique animals with similar values to those of another animal (offset for visual clarity). N=6-11 mice (3.5 month old) per group. * indicates $p<0.01$, # indicates $0.01<p<0.05$, and red line indicates mean. **(G-H)** Ovariectomized *ATRAID* KO mice have impaired bone strength responses to alendronate. Stiffness (G) and yield load (H) were analyzed by three-point bending test. Each circle represents an individual animal. Circles offset to the right represent unique animals with similar values to those of another animal (offset for visual clarity). N=6-11 mice per group. *indicates $p<0.01$, #indicates $0.01<p<0.05$, N.S., indicates not significant, and red line indicates mean.

Fig. 3. *ATRAID* is required cell-autonomously for N-BP inhibition of osteoclast prenylation.

(A) A serum marker of osteoclast activity is reduced in WT but not ATRAID KO ovariectomized mice by alendronate treatment. Serum CTX-I was measured by ELISA. Each circle represents an individual animal. Circles offset to the right represent unique animals with similar values to those of another animal (offset for visual clarity). N=8-13 mice per group. * indicates $p<0.05$. **(B)** Osteoclast histomorphometric responses are reduced in WT but not ATRAID KO ovariectomized mice by alendronate treatment. Osteoclast surface to bone surface ratio (Oc.S/BS) was determined by Tartrate Acid Phosphatase (TRAP)-assay reactivity. Each circle represents an individual animal. Circles offset to the right represent unique animals with similar values to those of another animal (offset for visual clarity). N=5-7 mice per group. * indicates $p<0.05$, n.s. indicates not significant, and red line indicates mean. **(C)** Quantitative PCR to examine mRNA expression of markers of osteoclast differentiation, *CTSK, RANK, TRAP,* in wild-type (WT) and $ATRAID^{KO}$ cells M-CSF enhanced, bone marrow macrophages (BMMs) differentiated with *RANKL* to osteoclasts. Expression is normalized to wild-type, undifferentiated BMM cells, using *ACTB* and *RPLP0* as control genes. Error bars represent the standard

deviation of technical triplicate reactions. **(D)** Percent of Annexin-V positive cells after a 48 hour alendronate treatment of differentiated *ATRAID* WT (+/+) and KO (-/-) BMMs into osteoclasts. Annexin V staining was assessed using flow cytometry. Each circle represents osteoclasts derived from an individual animal (split for treatment with 0, 10μM, 30μM alendronate). Red line indicates mean. * indicates $p<0.05$, N.S. indicates not significant. **(E)** Percent of Annexin-V positive cells after a 48 hour alendronate treatment in wild-type and *ATRAID*^{KO} differentiated RAW 264.7 osteoclasts. Annexin V staining was assessed using flow cytometry. Error bars represent the standard deviation of n=3 experiments (biological replicates), * indicates $p<0.05$. **(F)** Immunoblots of cell lysates of RAW wild-type (WT) and *ATRAID*^{KO} (KO) cells, and RAW 264.7-derived osteoclasts treated with alendronate for 48 hours, demonstrating *ATRAID* deficiency confers resistance to alendronate-induced prenylation defects. Top panel: immunoblot specific to the unprenylated version of Rap1a. Bottom panel: Gapdh, serving as a loading control. Alendronate concentrations were 0, 20μM, 80μM.

Fig. 4. *ATRAID* as a potential genetic factor for altered responses to nitrogen-containing bisphosphonates in patients. (A) Genome-wide studies of N-BP responsiveness in patients vs. cells. The outcomes considered from human studies involving N-BPs are: osteonecrosis of the jaw (ONJ), breast cancer bone marrow micrometastases (i.e., disseminated tumor cells (DTC)), and atypical femoral fractures (AFF). *ATRAID, ATR, CTC1, MINK1, ZBTB4* are statistically significant hits ($p < 0.05$) in N-BP CRISPRi screening, differentially expressed in both gene expression datasets (ONJ and DTC), and possess rare multiple non-synonymous coding variants in AFF cases but not controls. These five genes are visualized as the Venn diagram of overlap of lists of genes that met the following criteria: significant alendronate or zoledronate CRISPRi hits with absolute value of rho growth phenotype values >= 0.10 and p <= 0.05 (2357 out of 15851 genes) (*19*); differentially expressed N-BP in ONJ + DTC (774 out of 18415 for ONJ (*41*) and 20492 for DTC (*42*); multiple coding variant(s) in AFF cases and not

controls (1725 out of 13237 genes) (data as part of this study). **(B)** Patient genetic data for *ATRAID*. Raw expression values were normalized to 1 to fit on a comparable Y axis. * indicates $p<0.05$. N.S. indicates not significant. “X”-enriched refers to the fold-enrichment of the allele compared with a population with a similar genetic background as the cases. For example, for *ATRAID*, the D5G variant is present in 2 out of 28 AFF patients. Though this allele wasn’t detected in the 11 control samples, it is present in a population of European Americans (EA) that is representative of the study population at a prevalence of 0.015. Therefore, the D5G allele is (2/28) / 0.015 = 4.76X enriched in cases compared to the EA population. “v3” and “v2” refer to isoforms of the *ATRAID* gene. A simple binomial test was used to calculate the significance of each variant. * indicates $p<0.05$.

Supplementary Materials:

Fig. S1, related to Fig. 1. ATRAID is required for cellular responses to nitrogen-containing bisphosphonates. (A) Schematic of the exon structure of the three human ATRAID mRNA variants. The coding sequence for each variant is in green. Non-coding portions of each exon are in grey. The translated regions of variant 1 and variant 3 are shorter than variant 2 due to internal translation initiation sites. The location of the primer sets used to identify each ATRAID gene trap (GT) are indicated (in blue for ATRAID_GT1; in red for ATRAID_GT2). **(B)** mRNA analysis of ATRAID and GGPS1 expression levels in clones that contain independent gene-trap insertions in their respective loci. Wild-type KBM7 cells were compared with mutant alleles (labeled as GT) and GGPS1 was used as a loading control. **(C)** ATRAID-deficient cells are resistant to alendronate over a wide range of concentrations and cell numbers. KBM7 cell viability was determined by measuring cellular ATP levels and is expressed as a ratio of that compared with untreated cells. All measurements were performed in quadruplicate (biological replicates). * indicates $p<0.05$, unpaired t-test. **(D)** ATRAID overexpression sensitizes cells to alendronate. HEK-293T cells were transfected with either Metap2 (control), or ATRAID-cDNA

expressing vectors and the indicated doses of alendronate for 72 hours. Viability measurements were performed in quadruplicate (biological replicates). * indicates $p<0.05$, unpaired t-test. **(E)** Alendronate regulation of viability is dependent on ATRAID membrane targeting. Cells deficient in ATRAID (ATRAID_GT2) were transformed to express exogenous Metap2 (control), tubulin (control), ATRAID variant 2 (_v2), or ATRAID variant 2 lacking the transmembrane domain (Δmem_v2). Cells were treated with alendronate at the indicated dose for 72 hours. Cell viability was determined as in $p<0.05$, unpaired t-test (n=6) (3 biological replicates, 3 technical replicates). **(F)** An additional cell line whose alendronate-dependent regulation of prenylation requires ATRAID. Wild-type control and ATRAID-deficient KBM7 cells exogenously expressing or not expressing ATRAID cDNA were treated with the indicated dose of alendronate for 24 hours then lysed and analyzed by immunoblotting for the indicated proteins. Equal amounts of protein were loaded in each lane. This experiment was repeated three times (biological replicates) and was consistent all three times.

Fig. S2, related to Fig. 2. ATRAID is required for organismal responses to nitrogen-containing bisphosphonates.

(A) Schematic of ATRAID targeted gene locus and genotyping strategy. ATRAID exon 3-exon 5 are targeted, i.e., flanked by LoxP sites. **(B)** Confirmation of deletion of protein-coding genomic DNA at the ATRAID gene locus. WT, wild-type at the ATRAID locus; het, heterozygous; KO, homozygous deletion. **(C)** ATRAID KO mice have reduced body weight compared with ATRAID wild-type WT (+/+) mice. N=6-13 for wild-type, N=7-14 for ATRAID KO mice. * indicates $p<0.05$. **(D)** Cells from ATRAID KO mice lack ATRAID mRNA. Tail fibroblast cells were analyzed for mRNA expression of ATRAID by RT-PCR and normalized to RPLP0 mRNA levels. Error bars indicate standard deviation for n=4 (biological replicates). * indicates $p<0.05$, unpaired t-test. **(E)** Cells from the tails of ATRAID KO animals are resistant to the cytotoxic effects of alendronate. All cells were treated with the indicated concentration of alendronate for 72 hours. Cell viability

was determined by measuring cellular ATP levels and is expressed as a ratio of that compared with untreated cells. All measurements were performed in quadruplicate (biological replicates). * indicates $p<0.05$, unpaired t-test. **(F)** ATRAID mRNA is undetectable in tibia of ATRAID knockout mice. Tibias were analyzed for ATRAID mRNA expression by RT-qPCR and normalized to RPLP0 mRNA levels. Error bars indicate standard deviation for n=4 (biological replicates). * indicates $p<0.05$, unpaired t-test. **(G)** Femurs from ATRAID KO mice are slightly smaller but grossly morphologically normal. Representative traverse μCT images at the femoral distal metaphysis from wild-type and ATRAID KO mice. Femur lengths in millimeters (mm) were based on μCT measurement. Error measurements are standard deviation for n=5-6 mice. * indicates $p<0.05$, unpaired t-test. **(H, I)** ATRAID KO mice bone microstructure isn't significantly altered. Femur trabeculae (H) and cortical (I) regions were analyzed by μCT. Each circle represents an individual animal. Circles offset to the right represent unique animals with similar values to those of another animal (offset for visual clarity). N=8-10 (2-month-old) mice per group. n.s. indicates not significant, unpaired t-test. **(J-L)** ATRAID KO mice have impaired bone strength. Stiffness (J), yield load (K), and post-yield displacement (L) were analyzed by three-point bending test. Each circle represents an individual animal. Circles offset to the right represent unique animals with similar values to those of another animal (offset for visual clarity). N=8-10 mice (2-month-old) per group. * indicates $p<0.05$, n.s. indicates not significant, unpaired t-test. **(M, N)** Markers of osteoclast function aren't significant different comparing ATRAID wild-type, WT (+/+) with knockout, KO (-/-) mice. (M) Serum C-terminal telopeptides of type I collagen (CTX-I) were measured in serum obtained from 3-month-old males using ELISA. Each circle represents an individual animal. Circles offset to the right represent unique animals with similar values to those of another animal (offset for visual clarity). N=6 mice per group. n.s. indicates not significant, unpaired t-test. (N) Osteoclast surface to bone surface ratio (Oc.S/BS) was determined by Tartrate Acid Phosphatase (TRAP)-assay reactivity. Each circle represents an individual animal. Circles offset to the right represent unique animals with similar values to

those of another animal (offset for visual clarity). N=6 mice per group. n.s. indicates not significant, unpaired t-test. **(O, P)** ATRAID KO mice have altered markers of osteoblast function. (O) Gla-Osteocalcin was measured in serum obtained from 3-month-old males using ELISA. Each circle represents an individual animal. Circles offset to the right represent unique animals with similar values to those of another animal (offset for visual clarity). N=7-9 mice per group. * indicates $p<0.05$, unpaired t-test. (P) bone formation rate (BFR/BS) determined by double labeling using calcein followed by alizarin red were analyzed histologically. Each circle represents an individual animal. Circles offset to the right represent unique animals with similar values to those of another animal (offset for visual clarity). N=5-7 mice per group. * indicates $p<0.05$, n.s. indicates not significant, unpaired t-test.

Fig. S3, related to Fig. 3. *ATRAID* required cell-autonomously for N-BP inhibition of osteoclast prenylation.

(A) Osteoclast numbers are reduced in WT but not ATRAID KO ovariectomized mice by alendronate treatment. The number of osteoclasts per bone surface (N.Oc/BS) were determined by Tartrate Acid Phosphatase (TRAP)-assay reactivity. Each circle represents an individual animal. Circles offset to the right represent unique animals with similar values to those of another animal (offset for visual clarity). N=5-7 mice per group. * indicates $p<0.05$, n.s. indicates not significant, and red line indicates mean. **(B, C)** Osteoblast function isn't significantly altered by alendronate in WT or *ATRAID* KO ovariectomized mice. Bone formation rate (BFR/BS) (B), and mineral apposition rate (MAR) (C), were determined by double labeling using Calcein followed by Alizarin Red were analyzed histologically. Each circle represents an individual animal. Circles offset to the right represent unique animals with similar values to those of another animal (offset for visual clarity). N=5-7 mice per group. * indicates $p<0.05$, n.s. indicates not significant, and red line indicates mean. **(D)** Schematic of the mouse *ATRAID* first coding

exon, indicating the CRISPR-induced mutations present in the two *ATRAID*^{KO} clones used in Fig. 3.

Figure 1

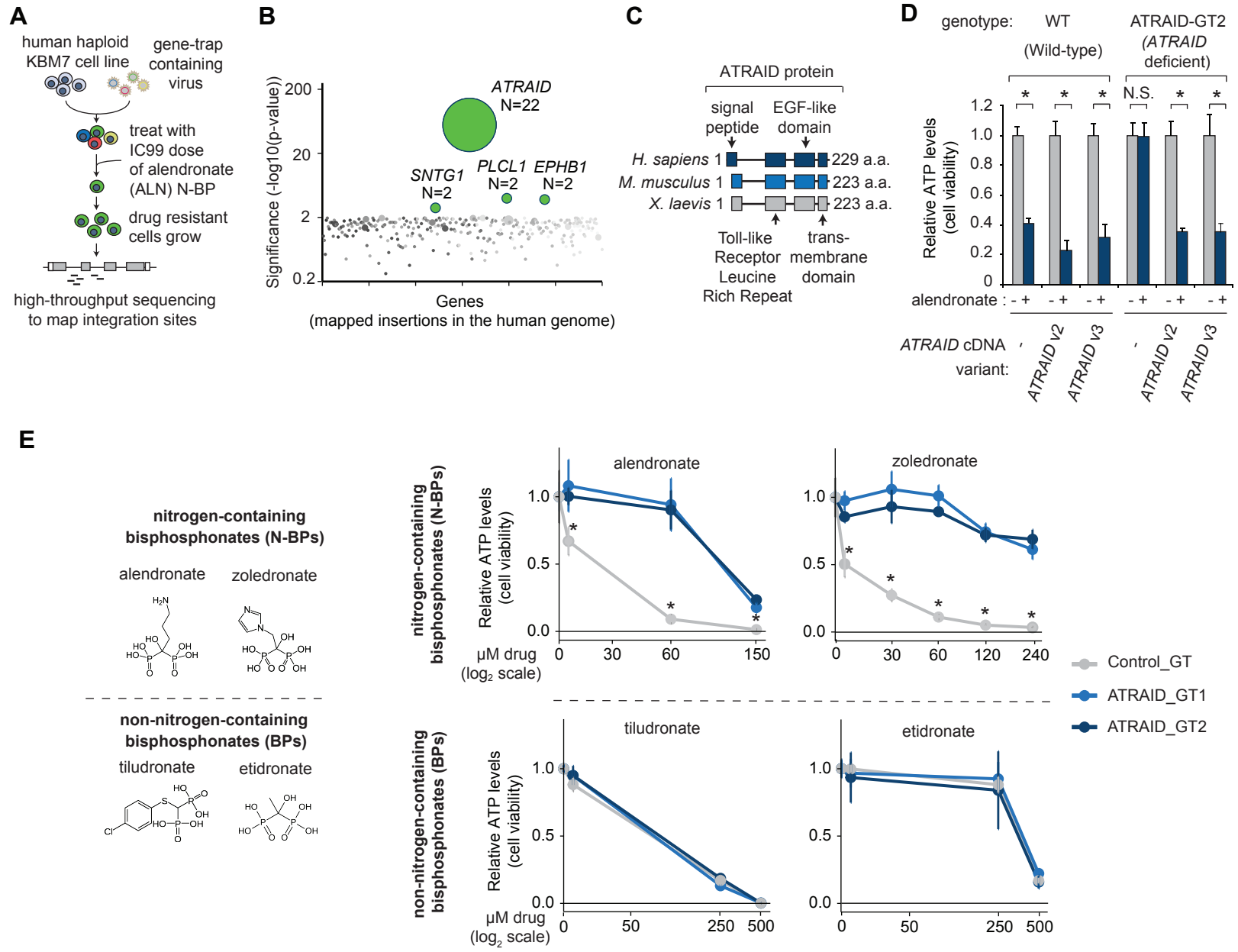
A
human haploid KBM7 cell line
gene-trap containing virus
treat with IC99 dose of alendronate (ALN) N-BP
drug resistant cells grow
high-throughput sequencing to map integration sites
B
Significance (-log10(p-value))
ATRAID N=22
SNTG1 N=2
PLCL1 N=2
EPHB1 N=2
Genes (mapped insertions in the human genome)
C
ATRAID protein
signal peptide
EGF-like domain
H. sapiens 1
M. musculus 1
X. laevis 1
229 a.a.
223 a.a.
223 a.a.
Toll-like Receptor Leucine Rich Repeat
trans-membrane domain
D
genotype:
WT (Wild-type)
ATRAID-GT2 (ATRAID deficient)
N.S.
Relative ATP levels (cell viability)
alendronate :
ATRAID cDNA variant:
ATRAID v2
ATRAID v3
E
nitrogen-containing bisphosphonates (N-BPs)
alendronate
zoledronate
non-nitrogen-containing bisphosphonates (BPs)
tiludronate
etidronate
nitrogen-containing bisphosphonates (N-BPs)
non-nitrogen-containing bisphosphonates (BPs)
Relative ATP levels (cell viability)
μM drug (log2 scale)
Control_GT
ATRAID_GT1
ATRAID_GT2
F
genotype:
ATRAID_KO (ATRAID deficient)
ATRAID cDNA variant:
v3
-
alendronate (μM):
(unprenylated) Rap1a
HDJ-2
unprenylated
prenylated
GAPDH
ATRAID-FLAG

Figure 2

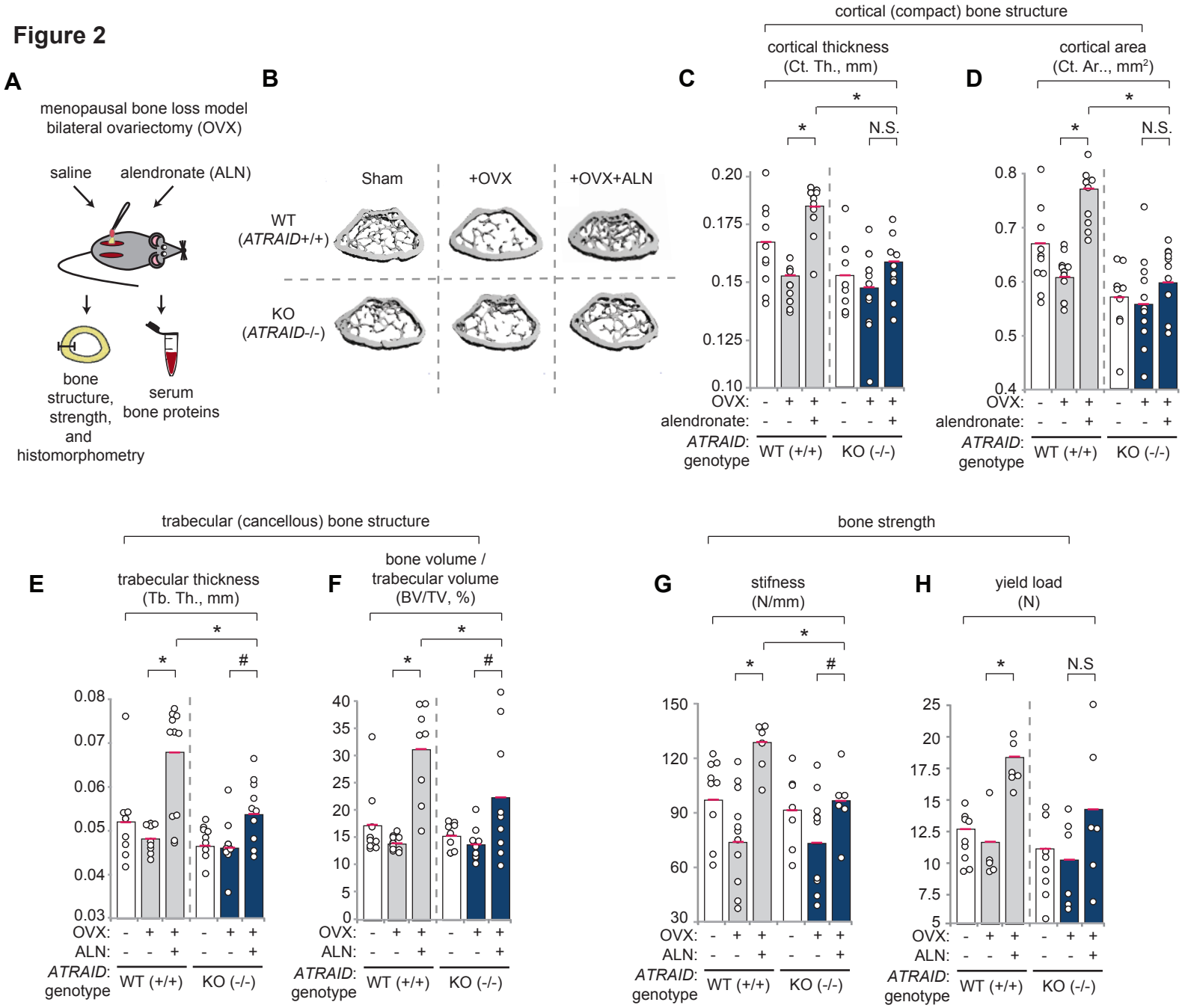
A
menopausal bone loss model
bilateral ovariectomy (OVX)
saline
alendronate (ALN)
bone structure, strength, and histomorphometry
serum bone proteins
B
Sham
+OVX
+OVX+ALN
WT (ATRAID+/+)
KO (ATRAID-/-)
C
cortical (compact) bone structure
cortical thickness (Ct. Th., mm)
D
cortical area (Ct. Ar.., mm²)
OVX:
alendronate:
ATRAID: genotype
WT (+/+)
KO (-/-)
N.S.
E
trabecular (cancellous) bone structure
trabecular thickness (Tb. Th., mm)
F
bone volume / trabecular volume (BV/TV, %)
ALN:
G
bone strength
stifness (N/mm)
H
yield load (N)

Figure 3

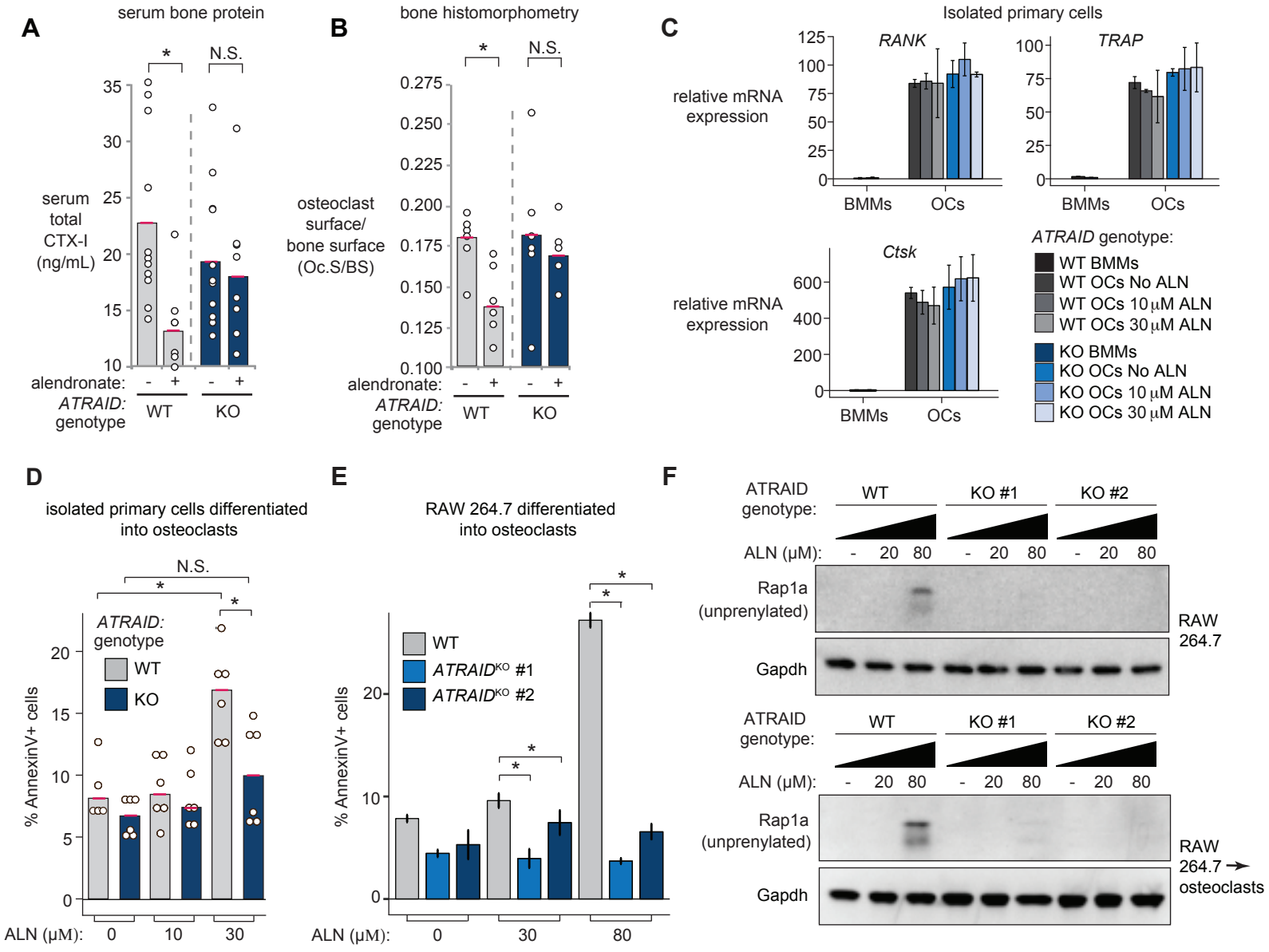
A
serum bone protein
serum total CTX-I (ng/mL)
alendronate:
ATRAID: genotype
WT
KO
N.S.
B
bone histomorphometry
osteoclast surface/ bone surface (Oc.S/BS)
C
Isolated primary cells
relative mRNA expression
RANK
TRAP
Ctsk
BMMs
OCs
ATRAID genotype:
WT BMMs
WT OCs No ALN
WT OCs 10 μM ALN
WT OCs 30 μM ALN
KO BMMs
KO OCs No ALN
KO OCs 10 μM ALN
KO OCs 30 μM ALN
D
isolated primary cells differentiated into osteoclasts
% AnnexinV+ cells
ALN (μM):
E
RAW 264.7 differentiated into osteoclasts
ATRAID^KO #1
ATRAID^KO #2
F
ATRAID genotype:
KO #1
KO #2
Rap1a (unprenylated)
Gapdh
RAW 264.7
RAW 264.7 → osteoclasts

Figure 4

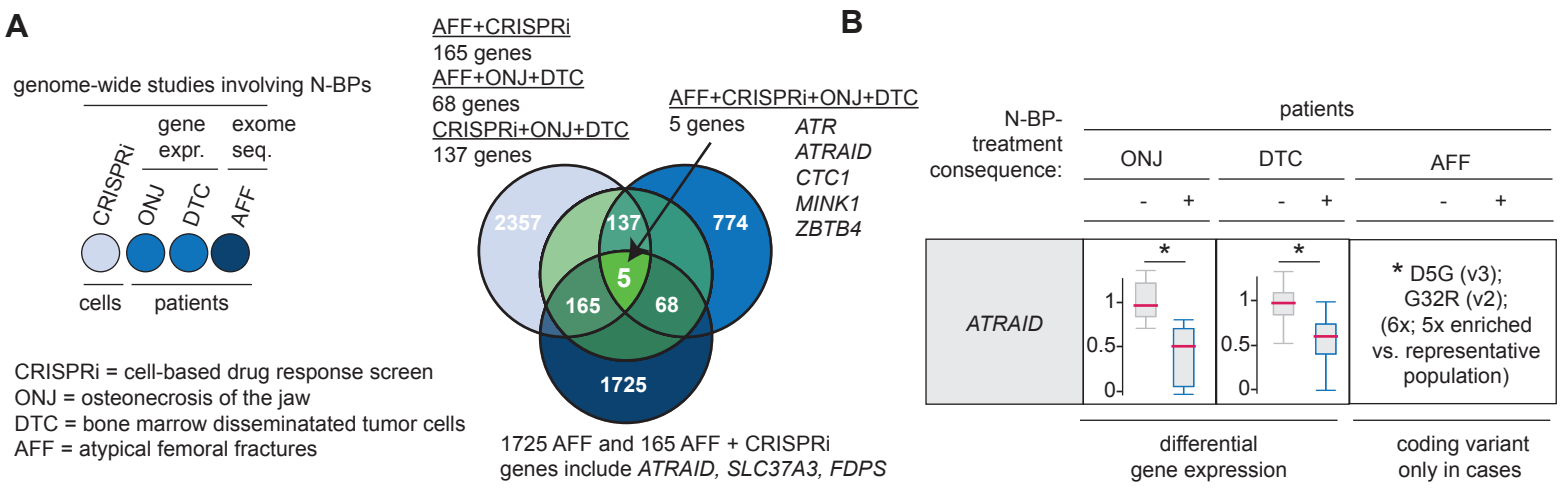
A
genome-wide studies involving N-BPs
gene expr.
exome seq.
CRISPRi
ONJ
DTC
AFF
cells
patients
CRISPRi = cell-based drug response screen
ONJ = osteonecrosis of the jaw
DTC = bone marrow disseminatated tumor cells
AFF = atypical femoral fractures
AFF+CRISPRi
165 genes
AFF+ONJ+DTC
68 genes
CRISPRi+ONJ+DTC
137 genes
AFF+CRISPRi+ONJ+DTC
5 genes
ATR
ATRAID
CTC1
MINK1
ZBTB4
2357
137
774
5
165
68
1725
1725 AFF and 165 AFF + CRISPRi genes include ATRAID, SLC37A3, FDPS
B
N-BP-treatment consequence:
patients
ONJ
DTC
AFF
-
+
ATRAID
*
1
0.5
0
* D5G (v3); G32R (v2); (6x; 5x enriched vs. representative population)
differential gene expression
coding variant only in cases

Figure S1

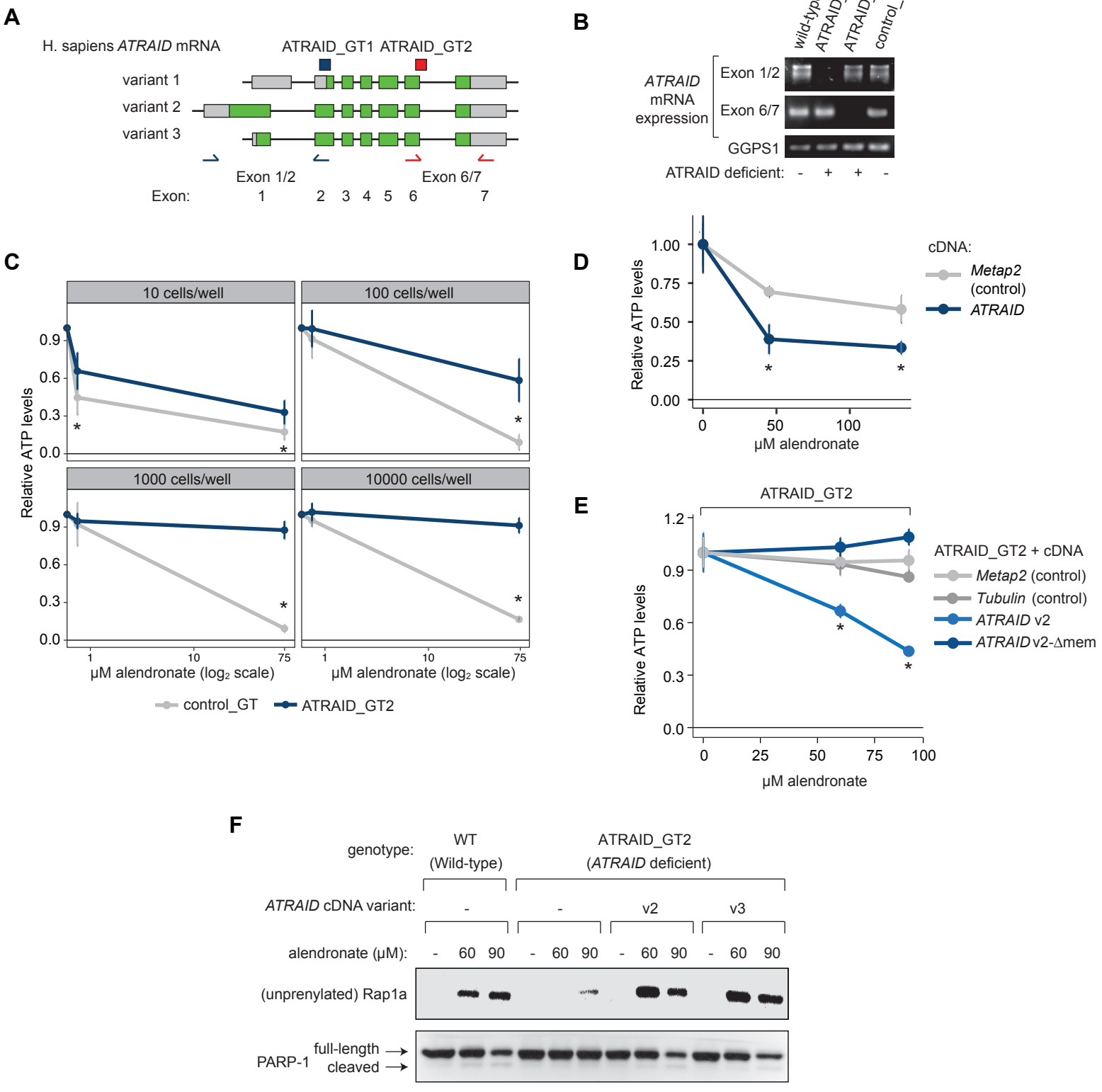
A
H. sapiens ATRAID mRNA
ATRAID_GT1 ATRAID_GT2
variant 1
variant 2
variant 3
Exon 1/2
Exon 6/7
Exon: 1 2 3 4 5 6 7
B
wild-type
ATRAID_GT1
ATRAID_GT2
control_GT1
ATRAID mRNA expression
Exon 1/2
Exon 6/7
GGPS1
ATRAID deficient: - + + -
C
10 cells/well
100 cells/well
1000 cells/well
10000 cells/well
Relative ATP levels
μM alendronate (log2 scale)
control_GT
ATRAID_GT2
D
Relative ATP levels
μM alendronate
cDNA:
Metap2 (control)
ATRAID
E
ATRAID_GT2
Relative ATP levels
μM alendronate
ATRAID_GT2 + cDNA
Metap2 (control)
Tubulin (control)
ATRAID v2
ATRAID v2-Δmem
F
genotype:
WT (Wild-type)
ATRAID_GT2 (ATRAID deficient)
ATRAID cDNA variant:
-
-
v2
v3
alendronate (μM):
- 60 90 - 60 90 - 60 90 - 60 90
(unprenylated) Rap1a
PARP-1
full-length
cleaved

Figure S2

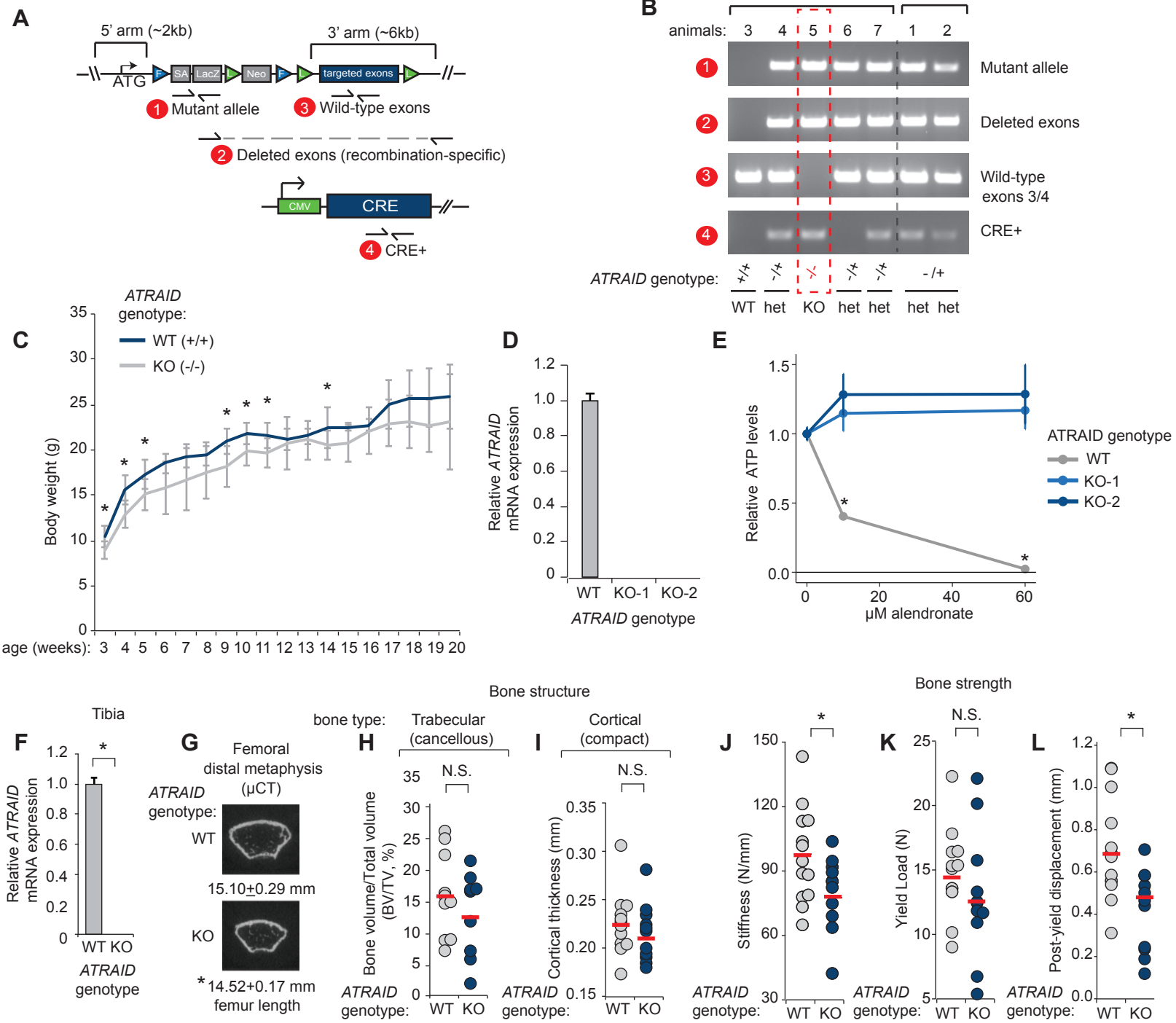
A
5' arm (~2kb)
3' arm (~6kb)
ATG
SA
LacZ
Neo
targeted exons
1 Mutant allele
3 Wild-type exons
2 Deleted exons (recombination-specific)
CMV
CRE
4 CRE+
B
Offspring (F1)
Parents
animals: 3 4 5 6 7 1 2
Mutant allele
Deleted exons
Wild-type exons 3/4
CRE+
ATRAID genotype: +/+ -/+ -/- -/+ -/+ - /+
WT het KO het het het het
C
ATRAID genotype:
WT (+/+)
KO (-/-)
Body weight (g)
age (weeks): 3 4 5 6 7 8 9 10 11 12 13 14 15 16 17 18 19 20
D
Relative ATRAID mRNA expression
WT KO-1 KO-2
ATRAID genotype
E
Relative ATP levels
μM alendronate
ATRAID genotype
WT
KO-1
KO-2
Tibia
F
Relative ATRAID mRNA expression
WT KO
ATRAID genotype
G
Femoral distal metaphysis (μCT)
ATRAID genotype:
WT
15.10±0.29 mm
KO
14.52±0.17 mm
femur length
Bone structure
bone type:
Trabecular (cancellous)
Cortical (compact)
H
N.S.
Bone volume/Total volume (BV/TV, %)
I
N.S.
Cortical thickness (mm)
Bone strength
J
Stiffness (N/mm)
K
N.S.
Yield Load (N)
L
Post-yield displacement (mm)
ATRAID genotype:
WT KO

Figure S2 (continued)

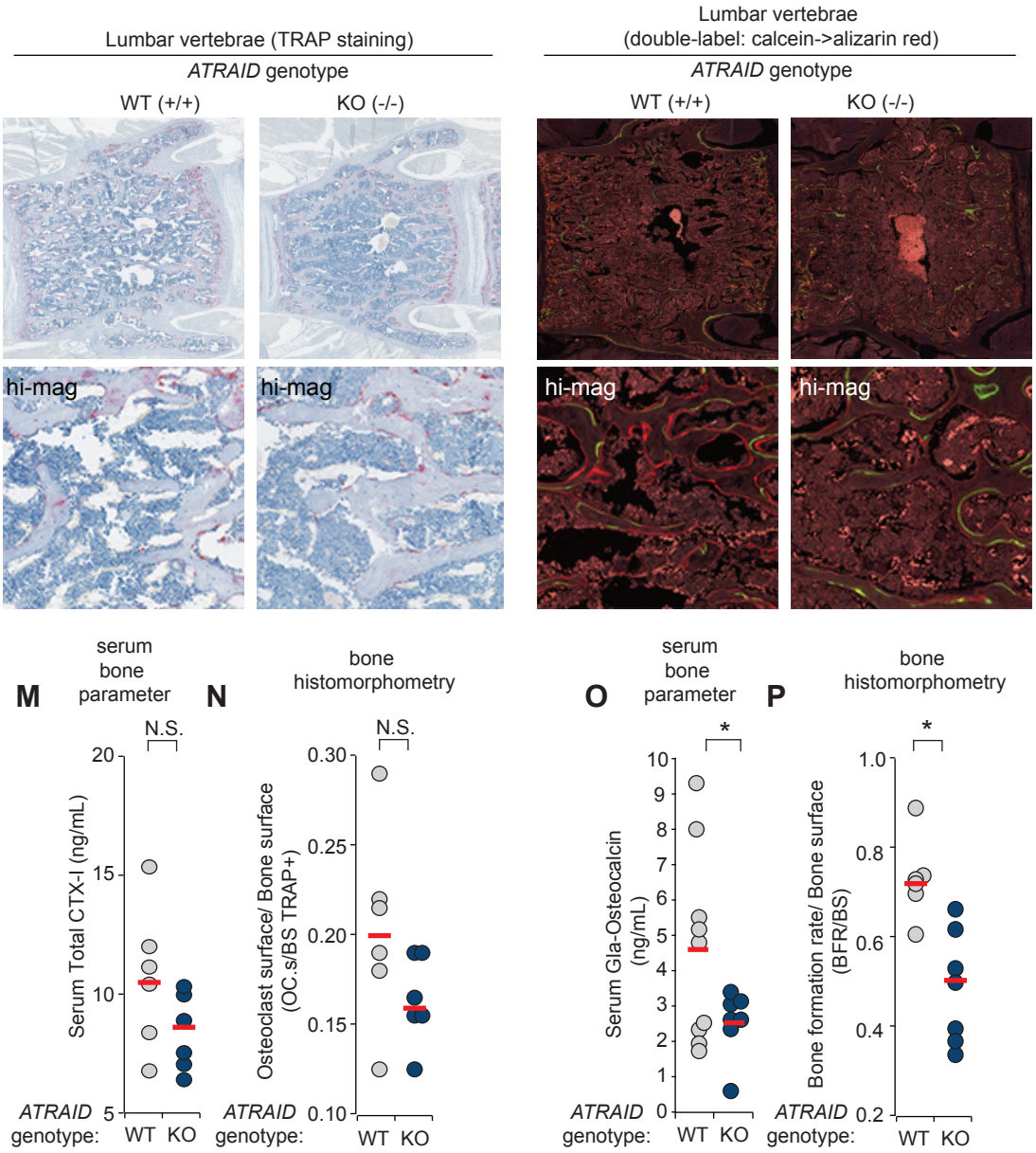

Figure S3

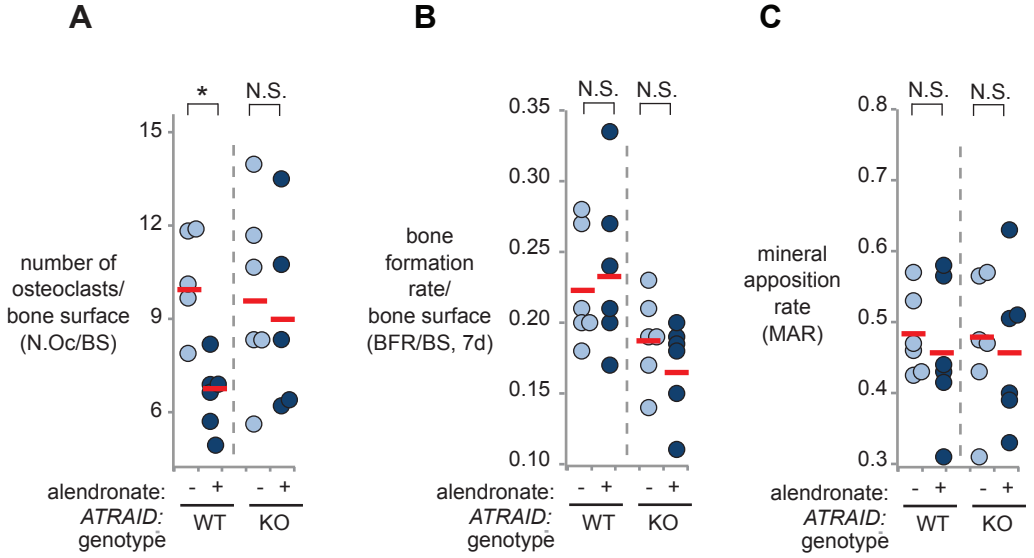
A
B
C
*
N.S.
number of osteoclasts/ bone surface (N.Oc/BS)
bone formation rate/ bone surface (BFR/BS, 7d)
mineral apposition rate (MAR)
alendronate: - + - +
ATRAID: genotype
WT
KO

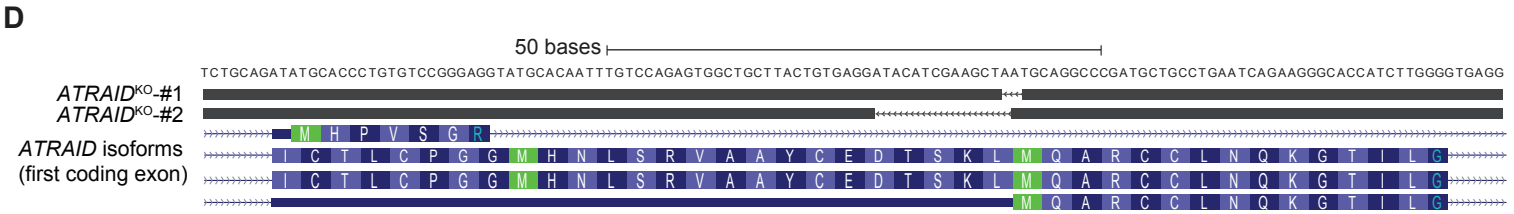
D
50 bases
TCTGCAGATATGCACCCTGTGTCCGGGAGGTATGCACAATTTGTCCAGAGTGGCTGCTTACTGTGAGGATACATCGAAGCTAATGCAGGCCCGATGCTGCCTGAATCAGAAGGGCACCATCTTGGGGTGAGG
ATRAID^KO-#1
ATRAID^KO-#2
ATRAID isoforms (first coding exon)